

Hydraulic fracturing

Authors: Kemal Yildizdag & Fabian Weber & Prof. Dr. habil. Heinz Konietzky, (TU Bergakademie Freiberg, Geotechnical Institute)

1	Theoretical background	4
1.1	Introduction to hydraulic fracturing.....	4
1.2	Governing equations	5
1.3	Mechanics of hydraulic fracturing	6
1.3.1	Continuum based failure conditions	6
1.3.2	Fracture initiation and borehole pressure.....	8
1.3.3	Fracture geometry.....	13
1.3.4	Fracture growth and orientation	17
1.4	Numerical simulation of hydraulic fracturing.....	20
2	Fracturing Technologies and Designs	26
2.1	Technical instruments and fracking materials.....	27
2.2	Wellbore completion design	31
2.3	Location and orientation of wellbore	37
2.4	Fracture placement design	38
3	Hydraulic fracture propagation in rock masses.....	43
4	References	51
5	51

Symbols

symbol	name of variable	unit
C	non-local kernel function	-
C_0	cohesion	MPa
D	substitution quantity	$\text{m}^3/\text{Pa} \cdot \text{s}$
E	Young's modulus	MPa
F	power-law fluid term	-
G	shear modulus	MPa
K_I	stress intensity factor	$\text{MPa}\sqrt{\text{m}}$
K_{IC}	fracture toughness	$\text{MPa}\sqrt{\text{m}}$
L	fluid leak-off term	-
N_ϕ	substitution quantity	-
Q_0	injection rate	m^3/s
R	fracture radius	m
V	fracture volume	m^3
c	proppant volumetric concentration	%
f	breakdown pressure model function	-
g	breakdown pressure model function	-
\mathbf{g}	gravity vector	m/s^2
h	hardening parameter	-
h_0	breakdown pressure model function	-
h_a	breakdown pressure model function	-
h_f	fracture height	m
k	permeability	m^2
l_c	zone length	m
p	fluid pressure	MPa
p_f	pore pressure in fracture	MPa
p_p	pore pressure in rock mass	MPa
p_{prop}	propagation pressure	MPa
p_w	wellbore pressure	MPa
p_{wf}	breakdown pressure	MPa
q	time dependent flow rate	m^3/s
r_w	wellbore radius	m
t	time	s
\mathbf{v}^p	proppant velocity vector	m/s
w	fracture width	m
w_0	maximum fracture opening	m
x	x-position Cartesian coordinate system	m
x_f	fracture half-length	m
y	y-position Cartesian coordinate system	m
z	z-position Cartesian coordinate system	m

symbol	name of variable	unit
Ω	fracture region	-
α	Biot's coefficient	-
γ	effective stress coefficient	-
ε	strain	-
ε_e	elastic strain	-
ε_p	plastic strain	-
ϑ	angular position, fracture angle	°
δ	Dirac delta function	-
$\delta\varepsilon$	strain increment	-
μ	fluid viscosity	Pa · s
ν	Poisson's ratio	-
ρ	fluid density	kg/m ³
σ	stress	MPa
σ_1	maximum principal stress	MPa
σ_2	intermediate principal stress	MPa
σ_3	minimum principal stress	MPa
σ_c	closure stress	MPa
σ_{C0}	substitution quantity	MPa
σ_{eff}	effective stress	MPa
σ_H	maximum horizontal stress	MPa
σ_h	minimum horizontal stress	MPa
σ_n	normal stress	MPa
σ_r	radial stress	MPa
σ_t	tensile strength	MPa
σ_V	vertical stress	MPa
$\sigma_x, \sigma_y, \sigma_z$	stresses in Cartesian coordinates	MPa
$\sigma_{\vartheta\vartheta}, \sigma_{z\vartheta}, \sigma_{r\vartheta}$	stresses in cylindrical coordinates	MPa
τ	shear stress	MPa
τ_{max}	critical shear stress	MPa
τ_x, τ_y, τ_z	shear stresses in Cartesian coordinates	MPa
$\tau_{\vartheta\vartheta}, \tau_{z\vartheta}, \tau_{r\vartheta}$	shear stresses in cylindrical coordinates	MPa
φ	friction angle	°
ϕ	porosity	%

1 Theoretical background

1.1 Introduction to hydraulic fracturing

Hydraulic fracturing is a key element for petroleum engineering since more than 50 years, but also applied in mining and geotechnical engineering. Within the last years this technique became even more important due to the application in geothermal projects and shale gas exploitation.

Today hydraulic fracturing is mainly applied to fulfil the following tasks:

- enhancement of rock permeability (e. g. petroleum engineering, geothermal energy)
- in-situ stress measurements and determination of hydraulic tensile strength
- de-stressing and de-gasification of rock masses during mining operations (e. g. coal mining)
- hydraulic disintegration / splitting of rock blocks (comminution)
- preconditioning of underground mine workings

The classical application of hydraulic fracturing consists in the injecting of a liquid usually called frac-fluid with high pressure along a selected section in a borehole (Donaldson, Waqi, & Nasrin, 2013). If the pressure is high enough, it creates one or more fractures extending into the surrounding rock (Yew & Weng, 2015). Pre-existing natural micro-fractures in the rocks could be extended due to the injection. Since the fractures acting as channels, the oil, gas or water flows through them into the wellbore. Conventionally it is assumed, that two fracture wings are created along the borehole during the fracking process. The propagation and orientation of these wings depend on the in situ stress field (see Figure 1). In most cases, fracture planes propagate perpendicular to the smallest principal stress σ_h (respectively σ_3) (Fjaer et al., 2008).

Once the fractures are generated and the fluid injection stops, the fractures are closing due to the acting closure stress σ_c , which could be roughly estimated as $\sigma_c \approx \sigma_3$ for isotropic rock mass. Taking into account anisotropic rock mass behaviour, this simplification is abrogated and the definition of closure pressure is more complex - see e. g. Iverson (1995) for further reading. However, for enhancing productivity, the channels should be kept open. In order to achieve this, proppants are injected during the pressurization process. Proppants are solids, which are mixed with the frac fluid

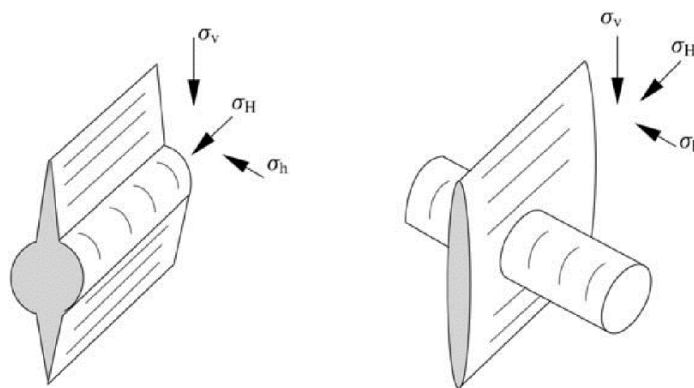


Figure 1 Different orientations of the fracture plane depending on the in situ principal stress directions (Fjaer et al. 2008).

and could be different in size and strength. Often used proppant are sand, sometimes coated, or special ceramic particles. An extensive overview about different proppants and their specific properties is given by Brown et al. (1992).

In the following chapters the most important aspects of hydraulic fracture mechanics are explained and discussed. At first common failure conditions for the rock mass and the initiation of fractures are described. Afterwards the pore pressure behaviour, fracture orientation and dimension, as well as different fracture models and the problem of stress shadows are presented. Furthermore, the governing equations for this multi-physics problem are explained and some numerical applications are shown.

1.2 Governing equations

According to Adachi et al. (2007) the basic equations of hydraulic fracturing are:

- (a) the elasticity equation,
- (b) the fluid flow equation,
- (c) the leak-off term,
- (d) the proppant transport equation,
- (e) the fracture growth condition.

Additionally, for modelling hydraulic fracture processes boundary and initial conditions are required as well as a mass conservation balance. The important relation between fracture opening w and fluid pressure p inside the fracture is given by the elasticity equation in integral form over the fracture region $\Omega(t)$ (Zhou & Hou, 2013):

$$C \cdot w = \int C(x, y) w(x, y, t) dx dy = p(x, y, t) - \sigma_c(x, y) \quad (1.1)$$

Where t is the time, C is the non-local kernel function containing the information about the media and σ_c is the closure stress. For a 3D plane fracture, the basic 2D fluid flow is governed by Reynold's equation (1.2) (Adachi, Siebrits, & Desroches, 2007):

$$\frac{\partial w}{\partial t} = \nabla \cdot [D(w)(\nabla p - \rho \mathbf{g})] + \delta(x, y) Q_0 + L + F \quad (1.2)$$

where $D(w) = w^3/12\mu$, μ is the fluid viscosity, ρ is the fluid density, \mathbf{g} the gravity vector, δ the Dirac delta function, Q_0 the injection rate, L the leak-off term and F the term for power-law fluids.

Terms for leak-off and power-law fluids will go beyond the scope of this chapter and are explained in (Adachi, Siebrits, & Desroches, 2007). The proppant volumetric concentration c in a fracture can be expressed by solving the advective mass conservation equation (1.3).

$$\frac{\partial(cw)}{\partial t} + \nabla \cdot (cw \mathbf{v}^p) = 0 \quad (1.3)$$

In Eq. (1.3) \mathbf{v}^p represents the proppant velocity vector. The propagation criterion can be expressed in several ways depending on the research topic and is a special type of tip boundary condition. They can be expressed via the relation between the stress intensity factor K_I and the fracture toughness K_{IC} (Adachi, Siebrits, & Desroches, 2007),

with stress singularities at the fracture tip (Adachi & Detournay, 2002) or via failure conditions (see Zhou et al. (2013) and Chapter 1.3.1). The boundary conditions are commonly given by zero fracture width and injection rate at the tip $x = x_f$ (Eq. (1.4), (1.5)) whereas the injection rate at the injection point $x = 0$ satisfies Eq. (1.6) (Savitski & Detournay, 2002).

$$w = 0, \quad x = x_f \quad (1.4)$$

$$q = 0, \quad x = x_f \quad (1.5)$$

$$q = Q_0, \quad x = 0 \quad (1.6)$$

where x represents the position and x_f the fracture half-length. The flow rate in dependence of position and time is given by q and the injection quantity by Q_0 . The initial conditions are given by Eq. (1.7) (Kovalyshen & Detournay, 2010).

$$x_f = w = q = 0, \quad t = 0 \quad (1.7)$$

Because of physical coherence, the mass conservation (1.8) for the fluid volume and fracture volume has to be fulfilled (Detournay, 2004).

$$2 \int_0^{x_f} w \, dx = Q_0 t \quad (1.8)$$

These are the governing equations for the problem of hydraulic fracturing. All these equations should be solved by considering hydro-mechanical coupling to obtain good approximations and realistic solutions. Specific assumptions are given for different fracture models (see Chapter 1.3.3) and so these governing equations are adapted for each model. In three dimensions the equations have to be solved numerically and fully coupled. Some Numerical results are shown in Chapter 1.4.

1.3 Mechanics of hydraulic fracturing

The hydro-mechanical coupled process of fracture initiation and propagation can be described by either classical continuum based theories (assuming critical constellations of stresses, energies or deformations) or fracture-mechanical based theories (assuming critical stress intensity factors, critical J-integrals, critical crack mouth openings). For very simple constellations analytical solutions can be obtained, otherwise different numerical simulation techniques have to be applied.

1.3.1 Continuum based failure conditions

Initiation of cracks in a rock during hydraulic fracturing plays an important role in order to open fluid channels. This means that the deformations in the rock are no longer elastic. The total strain increment $\delta\varepsilon$ thus could be divided into an elastic ($\delta\varepsilon_e$) and plastic part ($\delta\varepsilon_p$), see Eq. (1.9):

$$\delta\varepsilon = \delta\varepsilon_e + \delta\varepsilon_p \quad (1.9)$$

The plastic strain is irreversible and therefore, the deformation of rock remains over time after the removal of applied stress. The point at which plastic deformation of rock

occurs can be expressed by yield functions. These functions (e. g. Eq. (1.10)) are relations between stresses and a hardening parameter as given below:

$$f(\sigma_1, \sigma_2, \sigma_3, h) = 0 \quad (1.10)$$

where σ_1 , σ_2 and σ_3 are three principal stresses and h is the hardening parameter. The yield curve is described by h with the amount of plastic deformation of the material. The failure of rock is determined by different failure criteria. Two of them should be explained briefly, since they are essential for hydraulic fracturing.

Tensile failure

Most important for investigation of hydraulic fracturing is tensile failure, because brittle rocks mostly fail due to stresses (σ) exceeding the tensile strength σ_T of the material. Assuming that the compressive stresses have a positive sign, the criterion of failure can be written as:

$$\sigma < -\sigma_T. \quad (1.11)$$

However, hydraulic fracturing is also performed in porous media with pore pressure p_p . Therefore, the total stress is replaced by the effective stress. This transforms Eq. **Fehler! Verweisquelle konnte nicht gefunden werden.** into Eq. **Fehler! Verweisquelle konnte nicht gefunden werden.** with considering pore pressure.

$$\sigma - p_p < -\sigma_T \quad (1.12)$$

Eq. **Fehler! Verweisquelle konnte nicht gefunden werden.** is called the “maximum tensile stress criterion”. It indicates that as soon as the effective stress reaches the tensile strength, rock failure initiates.

Shear failure

Shear failure occurs at sufficiently high shear stresses generating two fracture planes moving relative to each other. It is a frictional process where the frictional force depends on the normal force pressing the two fracture planes together. Shear failure takes place if the critical shear stress τ_{max} is reached, depending on the normal stress σ_n . The equation for the failure criterion is shown in Eq. (1.13) called Mohr’s hypothesis.

$$|\tau_{max}| = f(\sigma_n) \quad (1.13)$$

Various shear failure criteria are possible for different types of failure envelopes. The simplest one is the failure criterion according to Tresca (Eq. **Fehler! Verweisquelle konnte nicht gefunden werden.**) by choosing a constant straight horizontal failure line in the τ - σ diagram.

$$\sigma_1 - \sigma_3 = 2C_0 \quad (1.14)$$

Rocks breaks down in shear whenever one half of the stress difference between the largest and smallest principal stress “ $(\sigma_1 - \sigma_3)/2$ ” reaches the cohesion value C_0 (also called inherent shear stress).

A more accurate description is the Mohr-Coulomb criterion. Since shear stress τ changes linearly with normal stress σ_n (Figure 2), the failure envelop is given by a straight line with slope φ (friction angle) and an intersecting point at C_0 . The relationship which describes the maximum shear stress when a rock fails is given by Eq. (1.15).

$$\tau_{\max} = C_0 + \tan \varphi (\sigma_n - p_p) \quad (1.15)$$

According to Eq. (1.15) shear failure is initiated if τ_{\max} is reached in the rock and it shows dependency on friction angle, effective stress and cohesion. In the principal stress space Eq. (1.15) can be expressed as:

$$\sigma_1 + p_p = \sigma_{C_0} + N_\varphi (\sigma_3 - p_p) \quad (1.16)$$

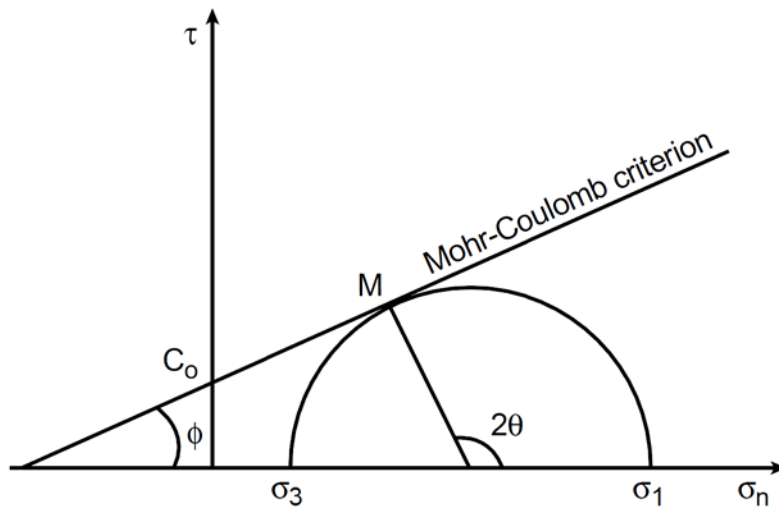


Figure 2 The τ - σ -diagram for the stress state of shear failure with marked Mohr-Coulomb criterion.

where σ_{C_0} and N_φ are:

$$N_\varphi = \tan^2 \left(\frac{\pi}{4} + \frac{\varphi}{2} \right) \quad (1.17)$$

$$\sigma_{C_0} = 2C_0 \sqrt{N_\varphi} \quad (1.18)$$

The rock breaks in shear if the stress state described by the fracture angle θ and the principal stresses σ_1 and σ_3 are situated on the Mohr-Coulomb failure line. This means in failure state the Mohr-circle touches the failure envelop. When the friction angle is 0° and 90° , the Mohr-Coulomb criterion transforms into the Tresca and Rankine criteria, respectively.

1.3.2 Fracture initiation and borehole pressure

For an accurate fracture design, borehole pressure and here especially the breakdown pressure is an important parameter. The breakdown pressure is the pressure at which fracture initiation in a rock starts. Furthermore, some geotechnical quantities can be determined from the breakdown pressure, for example the maximum horizontal stress

by inducing a vertical fracture in the rock mass (e. g. Konietzky et al. 1992 or (Gou, Morgenstern, & Scott, 1993). Nevertheless, this initiation process is highly complex and depends on several factors given below:

- (1) fracture fluid, fluid pressure and injection rate,
- (2) wellbore size and orientation,
- (3) in situ stress,
- (4) rock properties.

Regarding several influences on fracture initiation, a large number of breakdown models have been developed. Before investigating these models the stresses around the wellbore should be considered. The designation of the several stresses is according to Hossain, et al. (2000). Assuming a homogeneous, linearly elastic, isotropic rock mass the stresses around the wellbore could be expressed as Eq. (1.19) -

(1.23):

$$\sigma_r = p_p \quad (1.19)$$

$$\sigma_{\theta\theta} = \sigma_x + \sigma_y - 2(\sigma_x - \sigma_y) \cos 2\theta - p_w - 4\tau_{xy} \sin 2\theta \quad (1.20)$$

$$\sigma_{z\theta} = \sigma_z - 2\nu(\sigma_x - \sigma_y) \cos 2\theta - p_w - 4\nu\tau_{xy} \sin 2\theta \quad (1.21)$$

$$\tau_{r\theta} = \tau_{rz} = 0 \quad (1.22)$$

$$\tau_{\theta z} = 2(-\tau_{xz} \sin \theta + \tau_{yz} \cos \theta) \quad (1.23)$$

where: σ_r is the radial stress, $\sigma_{\theta\theta}$ is the tangential stress and $\sigma_{z\theta}$ is the axial stress at angular position θ on the wellbore.

The shear stresses τ_{xy} , τ_{yz} , τ_{zx} are acting on the wellbore in a rectangular coordinate system while $\tau_{r\theta}$, τ_{rz} , $\tau_{\theta z}$ are acting in a cylindrical coordinate system. The wellbore hydraulic pressure is marked by p_p , the angular position by θ . The stresses σ_x , σ_y , σ_z are normal stresses on the borehole. In Eq. (1.19) - (1.23) a single subscript means the direction of the stress. Stresses with two subscripts have to be interpreted as follows: the first index stands for the location of a stress on the plane which has an outward normal parallel to this axis and the second one stands for the direction where it acts along. For instance, the shear stress given by τ_{xy} acts on the plane x-axis with a direction to the y-axis. The distribution of the different stresses around the wellbore is depicted in Figure 3. A detailed explanation of the stresses in a rectangular coordinate system is given by Hossain, et al. (2000) and can be derived from the in situ principal stresses.

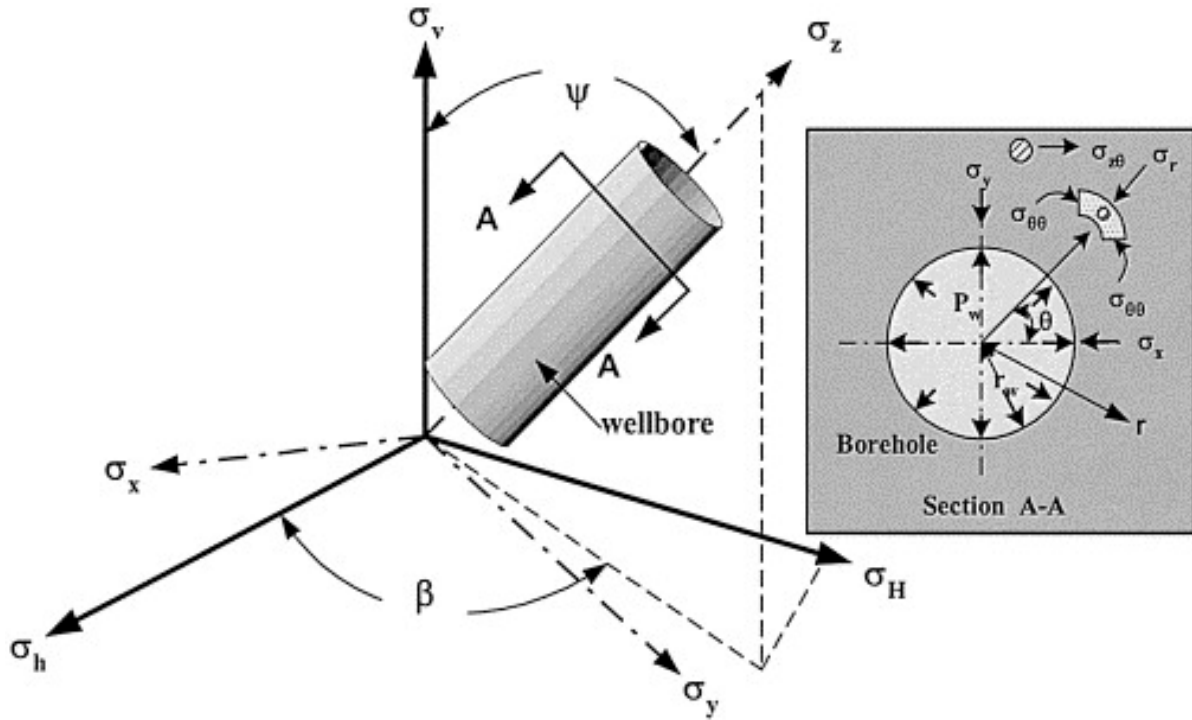


Figure 3 A random borehole in an in situ stress regime, stresses around the wellbore are displayed (Hossain, Rahman, & Rahman, 2000).

The fracture initiates for a non-perforated wellbore according to the failure criterion given in Eq. (1.11), when a principal tensile stress reaches the tensile strength of the rock. The three principal stresses can be calculated as follows:

$$\sigma_1 = \sigma_r \tag{1.24}$$

$$\sigma_2 = \frac{1}{2} \left[(\sigma_{\theta\theta} - \sigma_{z\theta}) + \sqrt{(\sigma_{\theta\theta} - \sigma_{z\theta})^2 + 4\tau_{\theta z}^2} \right] \tag{1.25}$$

$$\sigma_3 = \frac{1}{2} \left[(\sigma_{\theta\theta} - \sigma_{z\theta}) - \sqrt{(\sigma_{\theta\theta} - \sigma_{z\theta})^2 + 4\tau_{\theta z}^2} \right] \tag{1.26}$$

Stresses acting around an open vertical borehole in an impermeable rock are displayed in Figure 4. The highest stress is the vertical stress σ_v which remains constant in the rock. The stress σ_r first equals the wellbore pressure and then decays with distance from the borehole. For $\sigma_{\theta\theta}$ it is reverse, because it increases with higher distance. Both stresses are equal to the minimum horizontal stress in the far field. It is assumed, that pore pressure p_p is unaffected by the borehole pressure p_w .

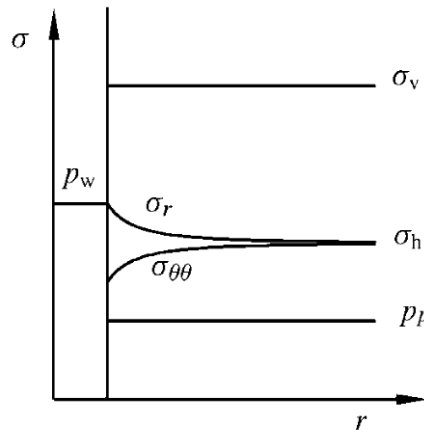


Figure 4 Stress distribution around a borehole assuming axisymmetric virgin stress field. The borehole is open, vertical and in an impermeable rock mass (modified from Fjaer et al. 2008).

As the compressive stresses have positive sign, the highest tensile stress is determined by the smallest negative principal stress. According to Equations (1.24) to (1.26) and Figure 4, σ_3 causes the highest tensile stress. By considering the pore pressure p_p , fracture initiation takes place in accordance to Eq. (1.12). As the principal stress σ_3 is related to $\sigma_{\theta\theta}$ and $\sigma_{z\theta}$, which are depend on p_w the breakdown pressure p_{wf} can be calculated by some mathematical re-arrangements. The obtained model for estimation of the breakdown pressure is called the “classic” or “conventional” breakdown model and is valid for a non-perforated vertical borehole (pre-conditions: $\psi = 0^\circ, \beta = 90^\circ, \theta = 0^\circ, \rightarrow$ Figure 3):

$$p_{wf} = 3\sigma_h - \sigma_H + \sigma_t - p_f. \tag{1.27}$$

The Equations for breakdown pressure in a horizontal borehole for different stress regimes are given by Hossain, et al. (2000) and will not be mentioned here. Equation (1.27) is based on the assumption that there is no fluid penetration into the formation. It is obvious that a changing pore pressure will influence the breakdown pressure. If the pore pressure increases the breakdown pressure decreases accordingly. Equation (1.27) characterizes an upper bound for the estimation of the initiation pressure. The lower boundary is expressed by Haimson’s model (Gou, Morgenstern, & Scott, 1993) and (Hossain, Rahman, & Rahman, 2000)):

$$p_{wf} = \frac{3\sigma_h - \sigma_H + \sigma_t - \alpha \frac{1-2\nu}{1-\nu} p_f}{2 - \alpha \frac{1-2\nu}{1-\nu}} \tag{1.28}$$

Where α is Biot’s coefficient and ν Poisson’s ratio. The model expressed by Eq. (1.28) takes Biot’s poroelastic theory into account which is explained e. g. by Dvorkin, et al. (1993).

According to Schmitt et al. (1989) the effective stress given by Terzaghi ($\sigma_{eff} = \sigma - p_f$) is not accurate enough so the “modified effective stress law” ($\sigma_{eff} = \sigma - \gamma p_f, 0 \leq \gamma \leq 1$) is introduced which formulates another breakdown model based on poroelasticity (Eq. (1.29)).

$$p_{wf} = \frac{3\sigma_h - \sigma_H + \sigma_t - \alpha \frac{1-2\nu}{1-\nu} p_f}{1 + \gamma - \alpha \frac{1-2\nu}{1-\nu}} \quad (1.29)$$

where γ indicates the effective stress coefficient.

The last model which is necessary to be introduced is the “fracture mechanics breakdown model” (Gou, Morgenstern, & Scott, 1993). In this model, the fracture initiates when unstable extension starts. The breakdown equation is derived under the assumption that the stress intensity factor is equal to fracture toughness ($K_I = K_{IC}$):

$$p_{wf} = \frac{1}{h_0(x_f, r_w) + h_a(x_f, r_w)} \left(\frac{K_{IC}}{\sqrt{r_w}} + \sigma_H f(x_f, r_w) + \sigma_h g(x_f, r_w) \right) \quad (1.30)$$

where x_f is the fracture length, r_w the well radius and h_0 , h_a , f , g are functions of x_f and r_w .

In literature several breakdown models are available, but Gou et al. (1993) have discovered that none of them could explain the complex breakdown process in detail. However, the authors discovered that fracture mechanical based approaches are promising. After examining the equations and relationships related to breakdown pressure, a sketch illustrating the borehole pressure development over time is shown in Figure 5.

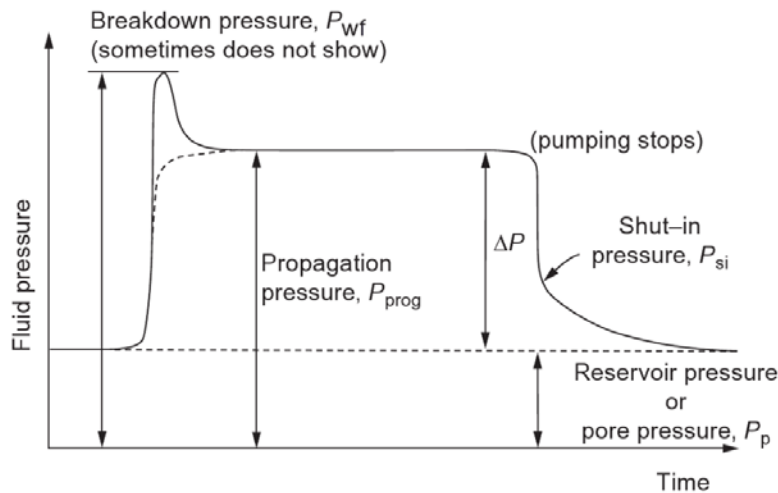


Figure 5 Schematic sketch of a borehole pressure record (modified from Yew, et al. 2015).

Before the injection starts, the downhole pressure equals the pore pressure of the surrounding rock mass. From the moment injection begins, the borehole pressure increases with time depending on the pumping rate up to the breakdown point. As mentioned before, the breakdown indicates the point at which fracture initiation occurs. The pressure drops and the fracture starts to propagate unstable, until pressure reaches a lower level at where the pressure is called propagation pressure p_{prog} (Yew & Weng, 2015). The fracture keeps on propagating from this state and possibly in a stable manner. The magnitude of propagation pressure commonly equals the minimum principal

stress. The pressure drops instantly when pumping stops and later decreases slowly with time. This sudden pressure drop can be explained by frictional pressure loss in the pipe, in the perforation entrance and at near-borehole area (Yew & Weng, 2015). The following slower decrease until the pore pressure of the rock mass is reached occurs due to fluid leak off. Same results and trends for the pressure obtained by numerical simulations are achieved by Wolgast & Konietzky (2014).

Figure 6 shows a more theoretical development of the borehole pressure p_w against pumped fluid volume V during two consecutive pumping cycles. Again the pressure increases in the first pumping cycle when injection starts. The linear slope is an indicator for elastic deformation until the breakdown pressure is reached. After the breakdown point the fracture volume grows at higher rate than the injection rate (unstable growing). The pressure drops then to the level of the propagation pressure. The second curve shows the pressure during a second pumping cycle. The same trends can be observed but the breakdown pressure is lower because the rock has been failed in tension and thus only resistance for further fracture propagation is the stress concentration around the borehole. The difference between the two breakdown pressures from these pumping cycles yields to the tensile strength of the surrounding rock mass. However, under real circumstances, the difference is not only related to tensile strength, because of smaller effective stress concentration owing to the fracture (Fjaer, Holt, Horsrud, Raaen, & Risnes, 2008).

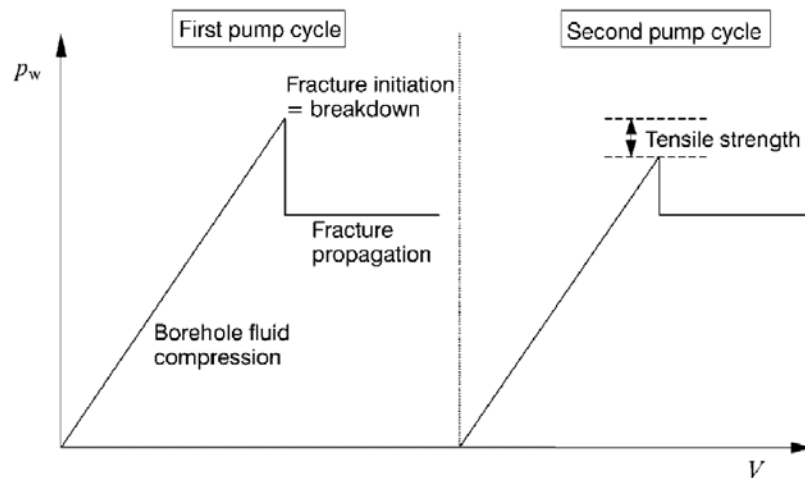


Figure 6 Wellbore pressure (theoretical) vs. fluid volume for a vertical borehole with two pumping cycles.

1.3.3 Fracture geometry

Fracture geometry is an important issue for the design of hydraulic fracture treatments. Values like maximum or average fracture width (aperture), borehole pressure, half-length and height of the fracture are important to get an insight into the processes within the stimulated reservoir. A detailed history of different hydraulic fracturing models is given by Adachi et al. (2007). The most common models are the Perkins-Kern-Nordgren (PKN), Khristianovic-Geertsma-de Klerk KGD, and circular fracture model.

The Perkins-Kern-Nordgren model (PKN)

This model was developed by Perkin et al. (1961) and later Nordgren (1972) who took fluid loss into account. The specific assumptions for this model are given in (Nordgren, 1972) and (Yew & Weng, 2015):

- (1) vertical fracture propagating in a straight line from the well,
- (2) restricted vertical height,
- (3) fracture is in plane strain in the vertical,
- (4) vertical cross-section has an elliptical form,
- (5) isotropic, homogeneous, linear elastic rock mass,
- (6) effect of fracture toughness on geometry is negligible.

Gravitational effects are not included in the model. The geometry of a PKN fracture is shown in Figure 7. The elliptical shape in the vertical and horizontal direction should be noticed, so the width is not constant along the fracture height and length.

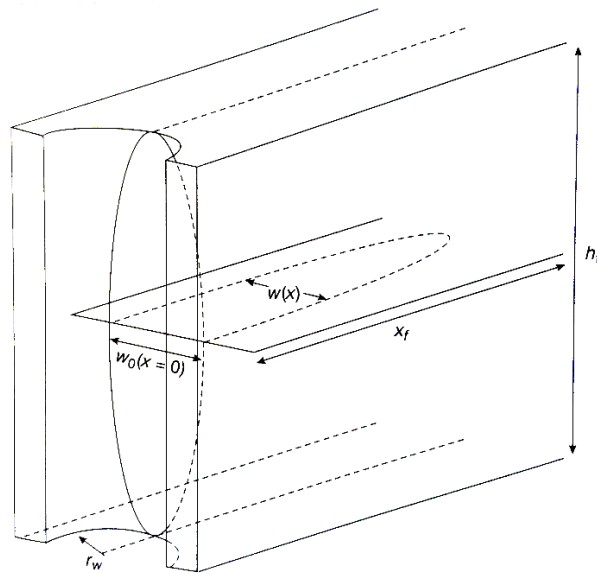


Figure 7 Perkins-Kern-Nordgren (PKN), model geometry (Valkó & Economides, 1995).

In Figure 7 the fracture width is marked by w and is a function of distance x from the wellbore. The maximum fracture width w_0 occurs at $x = 0$, where a fracture wing touches the wellbore. The fracture half-length is expressed by x_f , the fracture height by h_f and the wellbore radius by r_w . According to Nordgren (1972) and Yew et al. (2015) following equations for the PKN-model without fluid loss are obtained:

$$x_f = 0.68 \left(\frac{GQ_0^3}{(1-\nu)mh_f^4} \right)^{\frac{1}{5}} t^{\frac{4}{5}}, \quad (1.31)$$

$$w_0 = 2.5 \left[\frac{(1-\nu)\mu Q_0^2}{Gh_f} \right]^{\frac{1}{5}} t^{\frac{1}{5}} \quad (1.32)$$

$$p_w = \sigma_3 + 2.5 \left[\frac{G^4 \mu Q_0^2}{(1-\mu)^4 h_f^6} \right]^{\frac{1}{5}} t^{\frac{1}{5}} \quad (1.33)$$

where G is the shear modulus, Q the fluid injection rate, μ the fluid viscosity and t the time. If fluid loss is taken into account Eq. (1.31) - (1.33) are changing into other ones given by Yew et al., 2015. The PKN model gives good results for the stage of fracture where x_f is much larger than h_f ($x_f \gg h_f$) (Nordgren, 1972).

The Khristianovic-Geertsma-de Klerk model (KGD)

The second model used for hydraulic fracture predictions is the KGD model developed by Geertsma et al. (1969). The KGD model is valid under the assumptions listed below according to (Geertsma & de Klerk, 1969) and (Yew & Weng, 2015):

- (1) vertical fracture propagating in a straight line from the well,
- (2) restricted fracture height,
- (3) homogenous, isotropic, linear elastic rock mass,
- (4) purely viscous fluid in laminar flow regime,
- (5) geometric fracture-extension patterns are simple,
- (6) rectangular vertical cross-section of fracture,
- (7) plane strain conditions in the horizontal plane,
- (8) Barenblatt-shaped fracture tip.

A Barenblatt-fracture is a cusp-shaped crack. It is the only crack contour for which the released energy by a small contour change in the vicinity of a given point is zero (Barenblatt, 1961). This means only for such cracks the stress singularities of the linear elastic solution at the fracture tip are removed and equilibrium is reached (Barenblatt, 1961) and (Yew & Weng, 2015)). A sketch of the Barenblatt's contour condition for the fracture is shown in Figure 8.

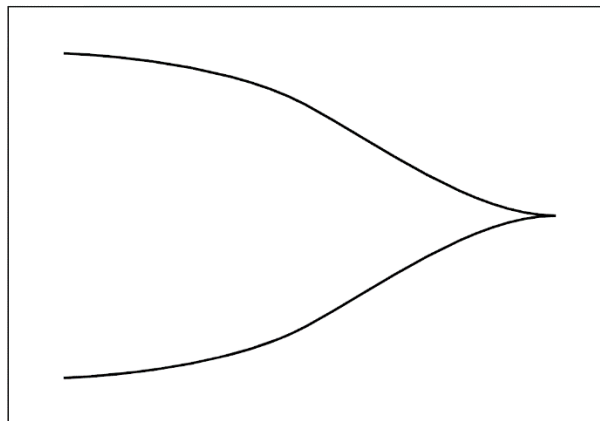


Figure 8 Barenblatt's contour condition for the fracture tip (Economides & Nolte, 2000).

The KGD fracture model is shown in Figure 9. The rectangular vertical cross-section should be noticed, and for the sake of simplicity the Barenblatt tip condition is not included in the figure. The nomenclature for the geometry elements of the fracture is the same as in the case of the PKN model. As for the PKN model, gravitational effects are not considered in the KGD model (Geertsma & de Klerk, 1969).

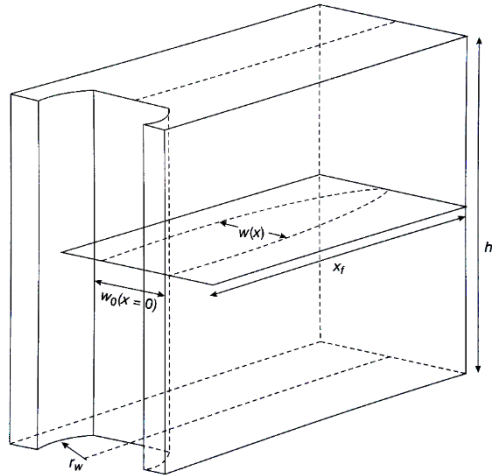


Figure 9 The Khristianovic-Geertsma-de Klerk (KGD) model geometry (Valkó & Economides, 1995).

If the fluid filled part of the fracture can be approximated by an ellipse and the dry zone (non-fluid filled part of the fracture) in the fracture tip is small, then the following solutions of the KGD model can be obtained in case of no leak-off ((Geertsma & de Klerk, 1969) and (Yew & Weng, 2015)):

$$x_f = 0.48 \left[\frac{8GQ_0^3}{(1-\nu)\mu h_f^4} \right]^{\frac{1}{6}} t^{\frac{2}{3}} \quad (1.34)$$

$$w_0 = 1.32 \left[\frac{8(1-\nu)\mu Q_0^3}{G} \right]^{\frac{1}{6}} t^{\frac{1}{3}} \quad (1.35)$$

$$p_w = \sigma_3 + 0.96 \left[\frac{2G^3\mu Q_0}{(1-\nu)^3 x_f^2} \right]^{\frac{1}{4}} \quad (1.36)$$

It should be noted that unlike the PKN model the wellbore pressure tends to decrease in time for the KGD model because of the inverse proportionality with respect to time. The KGD model gives good results for a fracture where the fracture length is much smaller than the fracture height ($x_f \ll h_f$) (Yew & Weng, 2015).

The circular fracture model

In some cases, for example when the minimum stress has a uniform vertical distribution, the shape of a hydraulic fracture might be circular. The governing equations for the KGD model can then be transformed to obtain the relations for the problem of a circular fracture ((Geertsma & de Klerk, 1969) and (Yew & Weng, 2015)). According to Savitski et al. (2002) some model assumption have to be mentioned:

- (1) axisymmetric hydraulic fracture propagation,
- (2) impermeable and homogenous linear elastic infinite medium,
- (3) Newtonian fluid is injected from a point source and reaches to the tip of the crack,

- (4) fracture propagates continuously in mobile equilibrium,
- (5) lubrication theory is applicable.

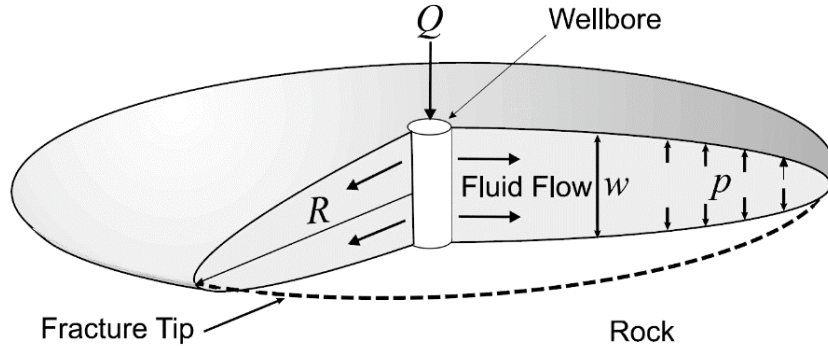


Figure 10 Circular hydraulic fracture (modified from Savitski, et al. 2002).

A sketch of the circular or penny-shaped fracture is shown in Figure 10. The approximate solutions for the fracture radius, maximum opening and wellbore pressure are given by Eq. (1.37) - (1.39) according to (Yew & Weng, 2015):

$$R = 0.548 \left(\frac{GQ_0^3}{\mu} \right)^{\frac{1}{9}} t^{\frac{4}{9}} \quad (1.37)$$

$$w_0 = 21 \left(\frac{\mu^2 Q_0^3}{G^2} \right)^{\frac{1}{9}} t^{\frac{1}{9}} \quad (1.38)$$

$$p_w = \sigma_3 - \frac{5}{4\pi} \frac{Gw_0}{R} \ln \left(\frac{r_w}{R} \right) \quad (1.39)$$

where r_w is the wellbore radius and R is the fracture radius.

1.3.4 Fracture growth and orientation

It is necessary to understand the evolution of fracture growth and orientation subsequent to the fracture initiation. All fractures related to hydraulic fracturing will grow in the direction of least resistance, which means that in some distance from the wellbore the fracture will propagate normal to the smallest principal stress σ_3 . In case of a formation where σ_3 is in horizontal direction (σ_h), at a vertical wellbore also vertical fractures will occur. Normally two fracture wings are generated extending in a σ_1 - σ_2 -plane (σ_V - σ_H -plane) parallel to the wellbore. For horizontal boreholes in the same stress regime $\sigma_V > \sigma_H > \sigma_h$ above statements for fracture growth are valid. However, the fracture is parallel to the borehole if the wellbore is drilled in σ_H -direction or perpendicular if the wellbore is drilled in σ_h -direction (Figure 1, Chapter 1.1) (Fjaer et al., 2008).

Wolgast & Konietzky (2014) found that the fracture orientation in the far field show a high dependency on the in situ stress regime. The authors obtained different computed fracture pattern depending on the in-situ principal stress ratio (Figure 11). In the 2D numerical model fluid is injected at a selected point (on the figure given by "IP 1"). For

a stress field with a stress ratio between σ_1 and σ_3 close to 1 fractures propagate nearly in all directions, whereas, if the anisotropic character between the stresses increases the fracture is more linear and elongated perpendicular to σ_3 . The modelling demonstrates, that significant anisotropy in stresses is necessary to create clear oriented fractures.

However, the fracture growth can also be limited by the vertical stress distribution and variation of elastic properties (Yew & Weng, 2015) or (Zeeb & Konietzky, 2014). In case of a layered rock mass associated stress or property rearrangements may restrict the fracture growth in height. Such layers in which the fracture could not propagate are called barriers. Furthermore, Warpinski et al. (1982) found that the stress contrast is the predominant factor for limiting the height growth of a hydraulic fracture. This means if the stress contrast between two layers is high enough the hydraulic fracture may not propagate through the one where higher stresses act. A sketch of hydraulic fracturing in a vertical wellbore with perforated holes and a limited fracture propagation due to the specific vertical stress distribution is shown in Figure 12.

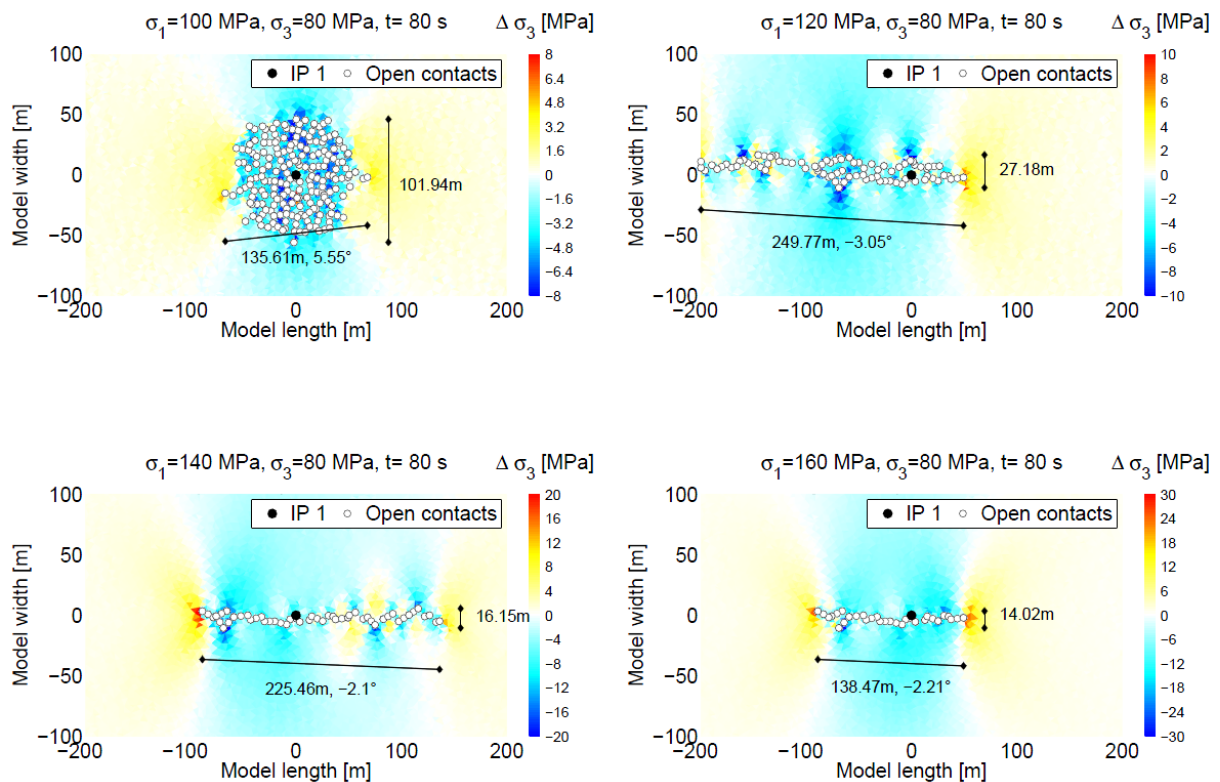


Figure 11 2D-fracture patterns for different in situ stress regimes (modified from Wolgast, et al. 2014).

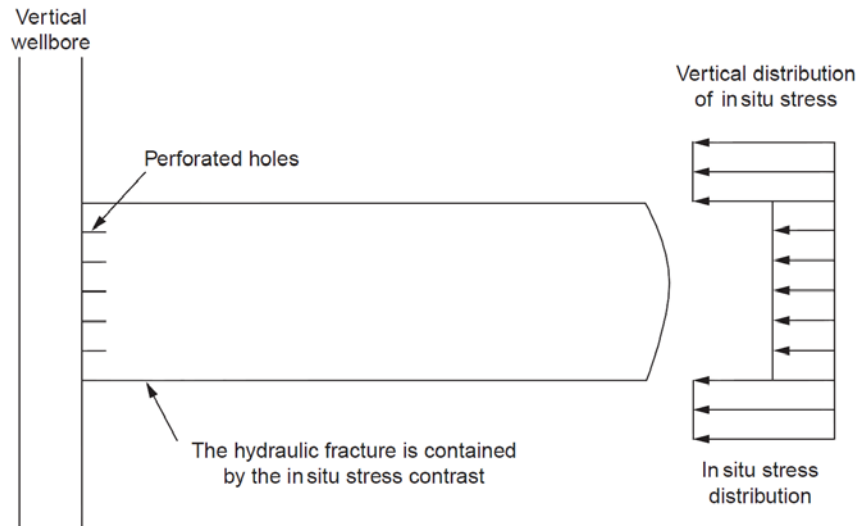


Figure 12 Hydraulic fracture constrained by a vertical in situ stress distribution (Yew & Weng, 2015).

As mentioned above, the vertical stress distribution is the dominant factor on propagation of hydraulic fractures amongst other factors such as rock properties. Elastic properties like Young's modulus E and Poisson ratio ν as well as permeability k , porosity ϕ and confining stress are factors affecting the length of a hydraulic fracture. Examples for this can be found in Zhou et al. (2013) and Adachi et al. (2007).

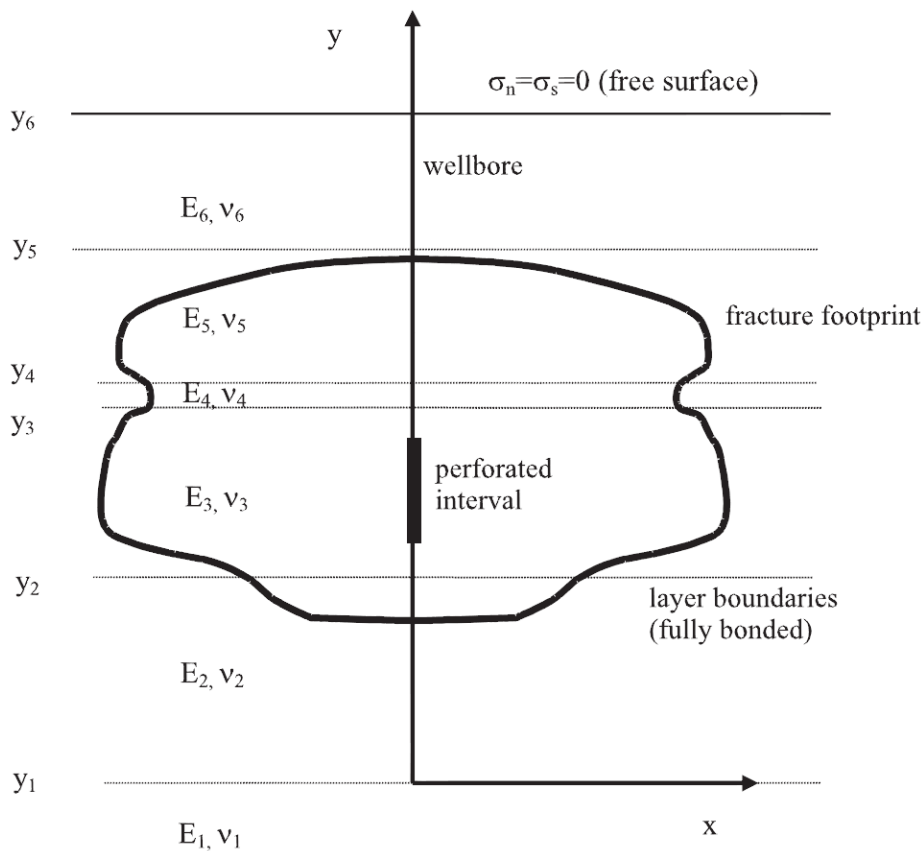


Figure 13 Fracture footprint in layered media with vertical property distributions (Adachi, Siebrits, & Desroches, 2007).

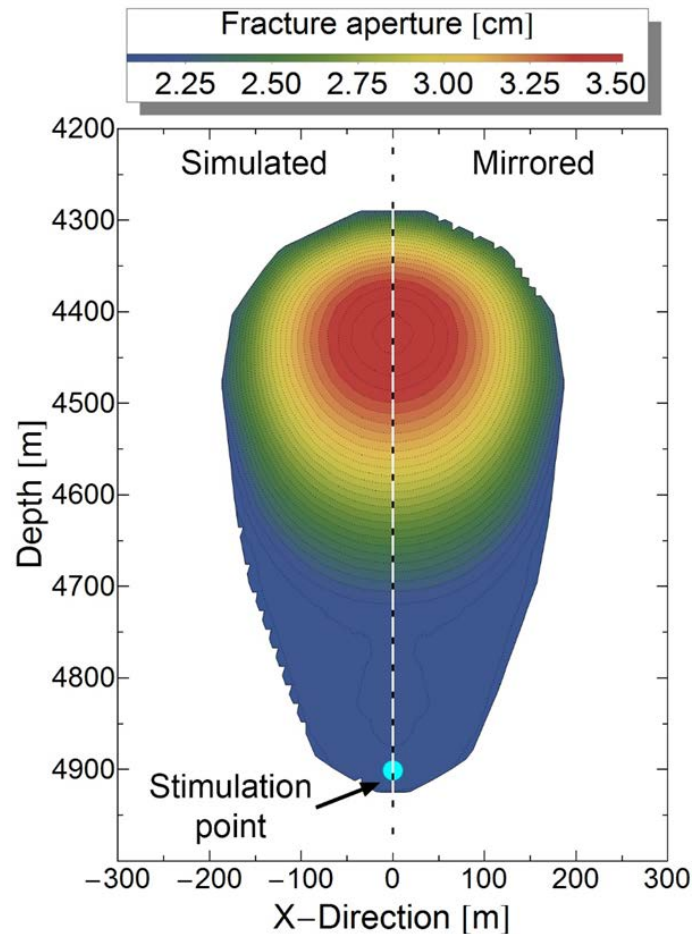


Figure 14 Hydraulic fracture propagating in rock mass under influence of gravity, fracture width is plotted (Zeeb, Wolgast & Konietzky, 2014).

Finally, the fracture growth and orientation in the far field mainly depends on the in situ stress regime, the orientation of the borehole within this regime, the rock properties and the acting gravity. For near field considerations the propagation process is more complex, for further reading a well description of the near field behaviour can be found in (Valkó et al., 1995).

1.4 Numerical simulation of hydraulic fracturing

Numerical calculations are used for problems where analytical solutions are not available such as for three dimensional hydraulic fracture propagation. The presented analytical models in Chapter 1.3.3 are useful approximations but may lead to inaccurate predictions in 3D. Generally, there are many different methods for modelling this kind of problems, e. g. FEM, XFEM, DEM or FDM, often coupled with CFD or SPH to take into account the fluid phase. Two of them will be introduced in this section, the discrete element method (DEM) and the finite difference method (FDM or VEM). Considering hydro-mechanical full coupling is strongly recommended during calculations by using these methods. A comprehensive overview about numerical methods applied in rock mechanics can be found in Jing (2003).

DEM modelling of hydraulic fractures

Zeeb & Konietzky (2014) and Zeeb, Wolgast & Konietzky (2014) conducted 3-dimensional numerical calculations by using the DEM-code 3DEC for hydraulic fracturing. At a specific injection point (block-contact region) a fluid flow is injected into the

model. The rock mass of the model is homogeneous, isotropic and impermeable for the fracturing fluid which is injected and therefore leak-off was neglected. The rock properties are given in Zeeb & Konietzky (2014) and the principal stresses follows $\sigma_H > \sigma_V > \sigma_h$. Gravitation is applied. Under the assumption of mirror symmetry only one half of the model was simulated to minimize the calculation time. A sketch of the model is shown in Figure 15. Depending on the material parameters, in situ stresses and the injection pressure, this fluid in-flow causes the water pressure in the surrounding contacts to increase, which leads to failure (opening) of the contacts and generates a fracture propagation along the block boundaries. Some important simulation results are depicted in Figure 16.

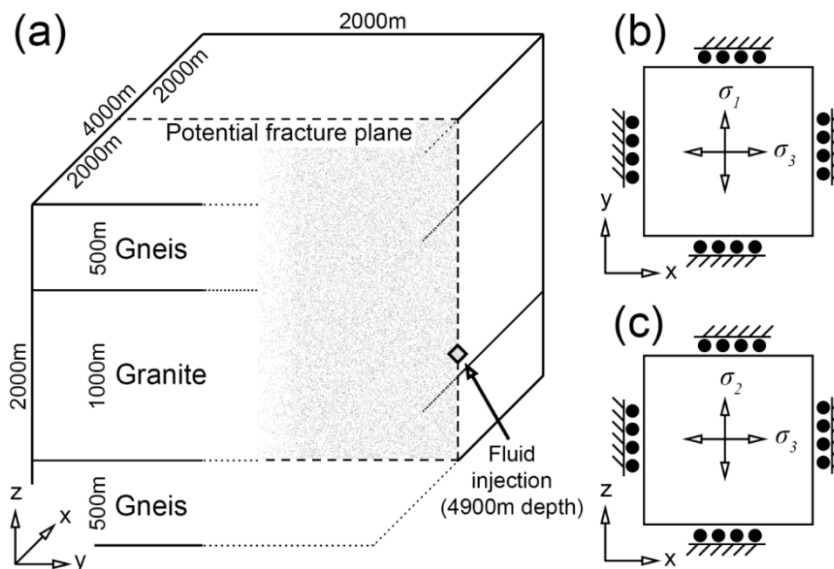


Figure 15 Model description for 3DEC: a) the layered rock mass, b) and c) roller boundary conditions and the action of principal stresses (Zeeb & Konietzky, 2014).

In Figure 16a, the evolution of fluid pressure and fracture aperture is shown. Every time the fluid pressure drops rapidly, the aperture drops accordingly, which indicates the failure of another contact in the model. Length and height of fracture evolves differently with time as shown in Figure 16b. The fracture propagates in direction of least stresses and due to the acting lithostatic pressure smaller stresses occur in smaller depths, so the fracture propagates easily along the vertical direction than along the horizontal direction. Figure 16c shows a spatial representation of the generated fracture. The fracture propagation causes an increase in tension in the areas parallel to the plane and a strong stress concentration at the fracture tip (Zeeb & Konietzky, 2014).

With the simulation of hydraulic fracturing by using the hydraulic fracture geometry, fluid pressure and fracture aperture can be well estimated. Based on these results researchers are able to make conclusions about the permeability increase and thus the productivity enhancement of the fracture treatment.

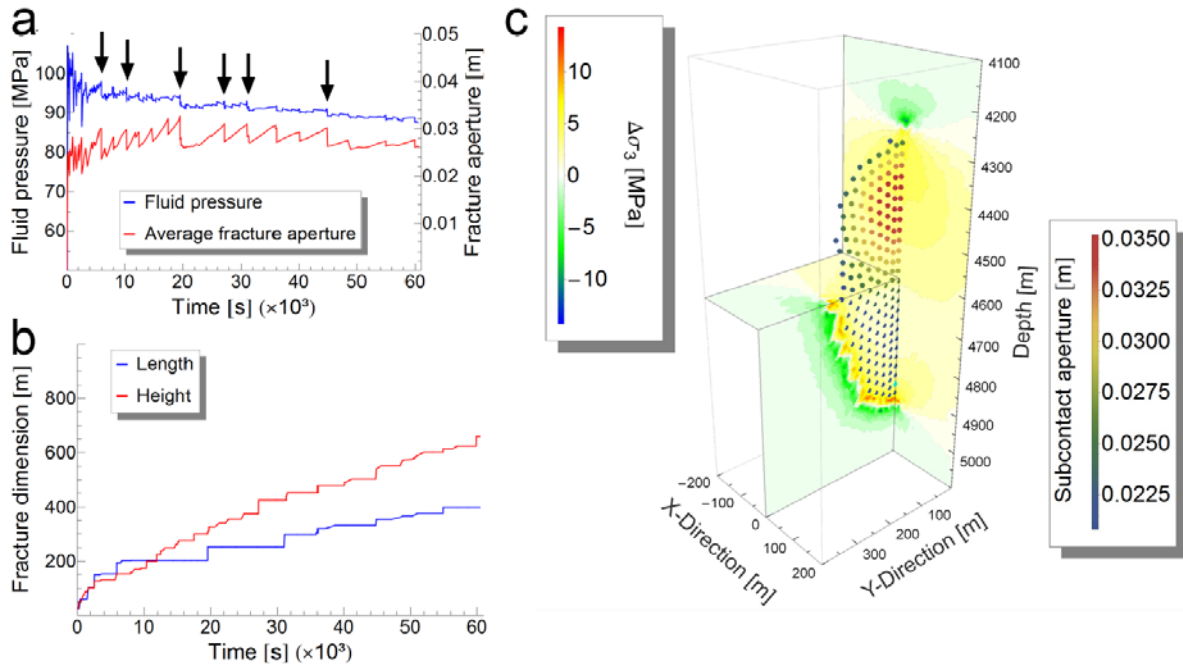


Figure 16 Results of the hydraulic fracture modelling with 3DEC: a) wellbore pressure and fracture aperture over time, b) fracture length and height over time and c) fracture geometry, aperture and the minimum principle stress change around the fracture (modified from Zeeb & Konietzky, 2014).

FDM modelling of hydraulic fractures

FDM has some shortcomings such as inflexibility in dealing with fractures, complex boundary conditions, irregular meshes and inhomogeneous material. Therefore, FDM method was coupled with the Finite Volume Method (FVM) to overcome these disadvantages. The FVM is also a direct approximation method but in the integral sense. With the help of FVM irregular meshes and complex boundary conditions can be used. Typical FDM and FVM grids are shown in Figure 17. However, in order to fulfil the necessary continuity of the grid, the order of shape functions along a common edge shared by two elements must be the same, so that no displacement discontinuity shall occur. The elements in the grid are represented by polyhedral elements (Jing, 2003).

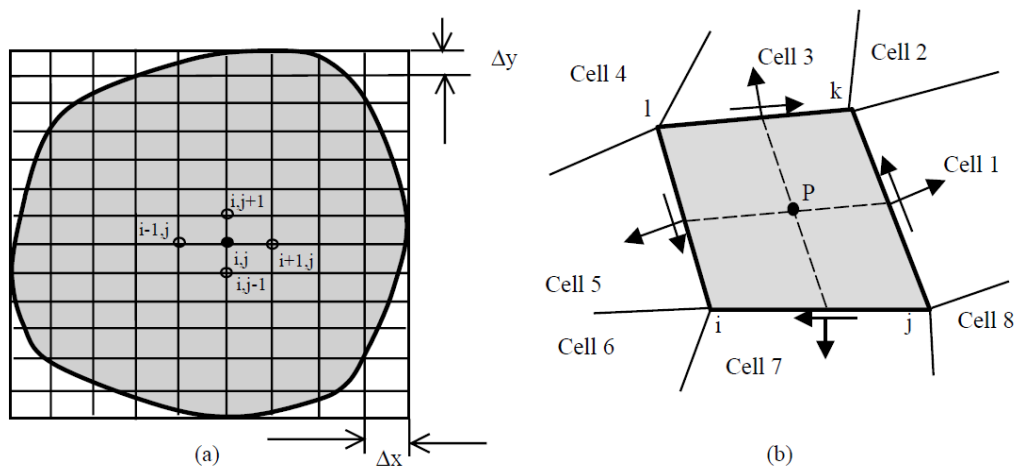


Figure 17 Different grids for a) FDM and b) FVM (Jing, 2003).

The fluid flow can be simulated through permeable solids, whereas a transient fluid flow analysis is conducted and thus pore pressure changes can occur (Itasca 2013).

Fluid flow equations are solved in the same way like mechanical equations by discretizing them via difference schemes. Thereby the pore pressures are calculated and stored in grid points and zone values are obtained by averaging. For modelling hydraulic fracturing, a hydro-mechanical coupling is necessary, where fluid and mechanical calculations are done in parallel because in this case changes in pore pressure influences deformations and volumetric strain causes the pore pressure to evoke (Itasca 2013).

For modelling hydraulic fracturing the generation of fractures is the basic concept. The solution for this challenge are virtual cracks, which are generated in failed zones of continuous media. The concept of virtual fractures is shown in Figure 180. The model consists of different elements (zones), if one zone fails either in tensile or shear the virtual fracture propagates within the zone and changes the zone length l_c due to pore pressure changes. This means that in case of purely tensile failure, the fracture width can be expressed as the displacement or strain at the nodes of the failure zone perpendicular to the fracture plane. In case of considering shear failure, the dilation of the rock enters the calculations of fracture width.

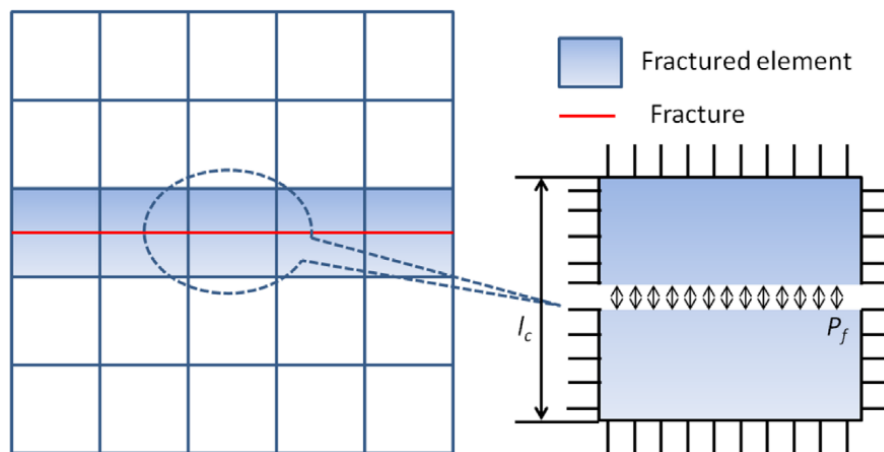


Figure 18 Principle of virtual fractures in continuous media (Zhou et al., 2014).

After solving the fracture issue in continuous media in principle, the numerical calculation of hydraulic fracturing is briefly explained. The same rock properties as used in the DEM simulation are considered in the continuous case. The main differences related between these two models are:

- (1) Gravity force is neglected,
- (2) smaller model,
- (3) no layered media (only one medium),
- (4) there is no symmetry, model is in full 3D and
- (5) slightly different principal stresses.

This means that the simulation results are not well comparable and show only the principles and opportunities of modelling hydraulic fracturing in different ways. The fluid is injected into one zone of the model and the calculations runs for about 400 seconds of injection. Figure 19 is a sketch of the model and gives the directions of the contained principal stresses along with boundary conditions. The virtual fracture concept is used for estimating the fracture width depending on the calculated displacements. Some calculation results are shown in Figure 20.

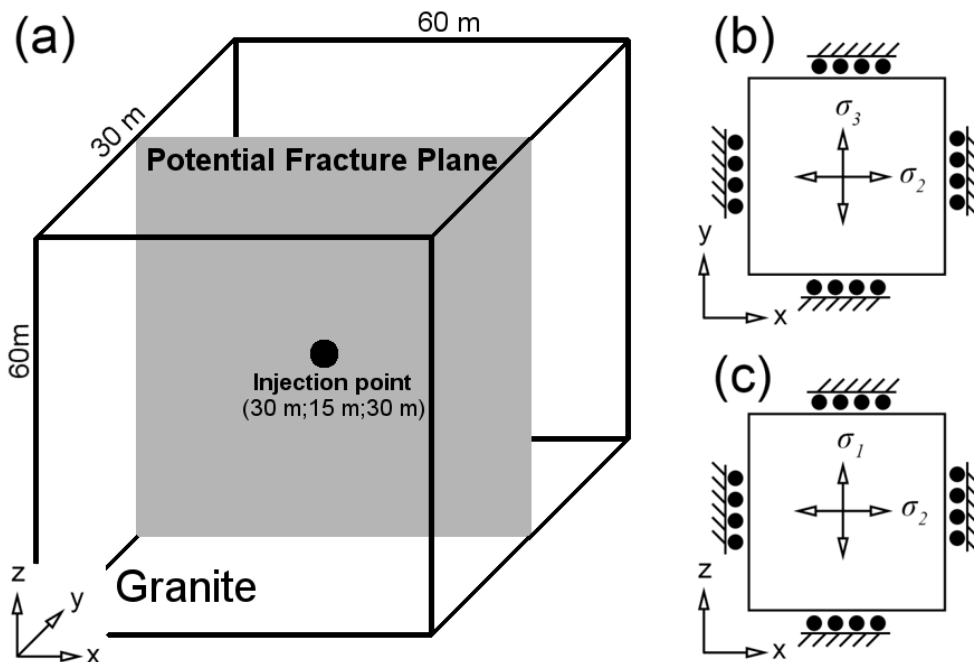


Figure 19 Model description: a) the rock mass and potential fracture plane, b) and c) boundary conditions and the action of principal stresses.

In Figure 20a, the failed zones and thus the fracture are visualized. The virtual crack propagates radial in the directions σ_1 and σ_2 with the injection zone at the centre. This is the proper propagation because no gravity acts on the model. The calculated permeability (Figure 20b) shows also a radial distribution with the highest permeability at the centre, shrinking with greater distance from the injection point. The fracture exhibits more or a less penny-shaped form. Figure 20c shows the pore pressure evolution at the injection point over time, it increases rapidly from the beginning of injection and it drops after reaching the breakdown pressure. The fracture height and half-length are shown in Figure 20d. A cross-section ($y = 15 \text{ m}$, $z = 30 \text{ m}$) of the fracture width is represented in Figure 20e with the highest opening at the injection point. The fracture width decreases with increasing distance from the injection zone due to the decreasing pore pressure beyond the injection point. Notice the correlation between permeability and fracture width.

Finally, there are several methods for adapting hydraulic fracturing into numerical simulations giving well approximations and results for this kind of problem. Nevertheless, different numerical methods and codes have advantages and shortcomings. Therefore, often couplings between solid-mechanical and fluid-mechanical techniques and codes, respectively, are applied. It is also necessary to mention that the grid size and discretization method have influence on the fracture simulation results, which makes a detailed model calibration inevitable.

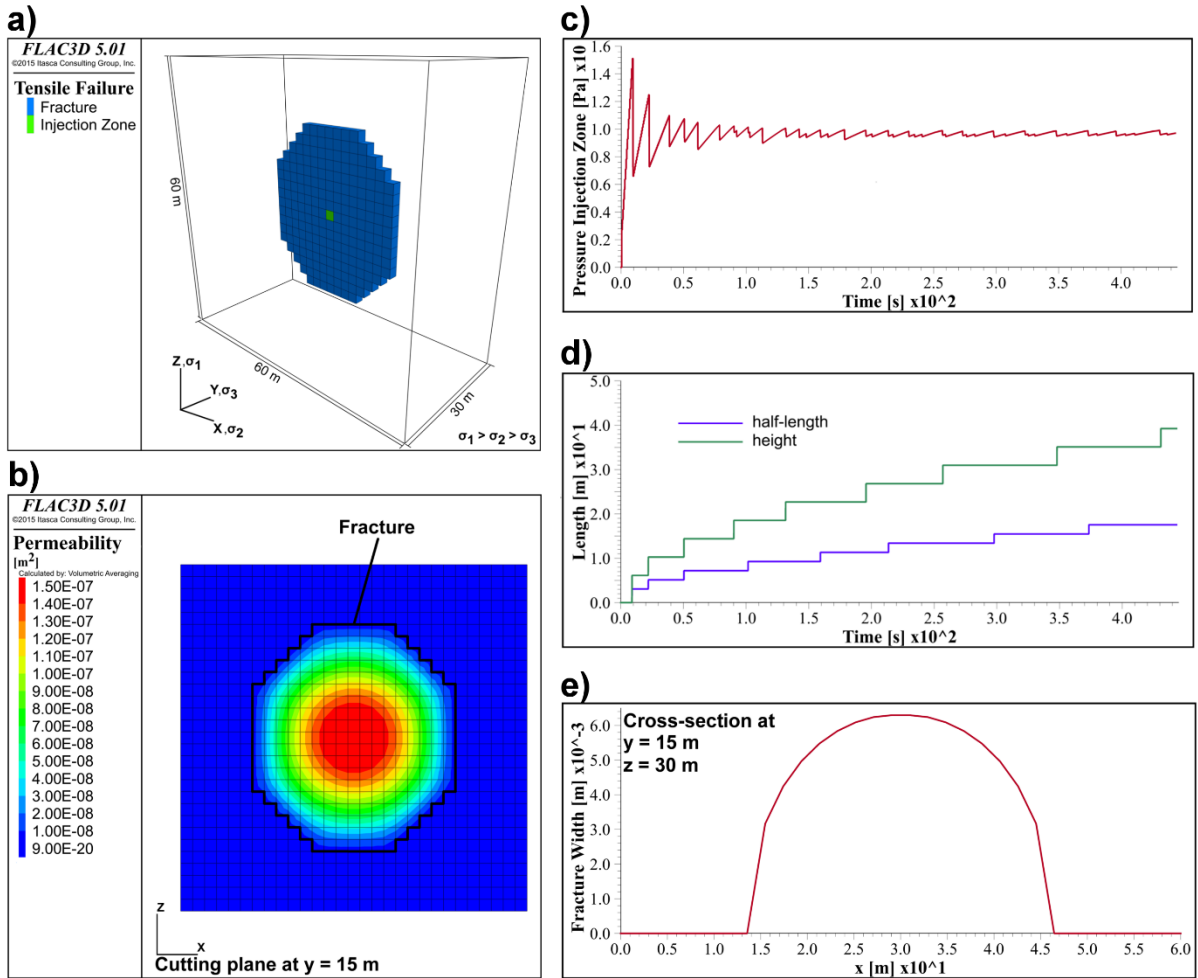


Figure 20 Results of FDM modelling: a) fracture geometry within the model, b) permeability distribution in the fracture, c) pore pressure evolution at injection point over time, d) fracture height and half-length evolution over time and e) cross-section of fracture width.

2 Fracturing Technologies and Designs

Typically, fracturing or stimulation is described as creating fractures by using several technologies (fluids, explosives etc.) at a rock which bears oil, gas or raw materials, to ease the flow between a reservoir and a wellbore by enhancing permeability. Relying on employed technology and reservoir characteristics, some more working steps such as using perforation tools, proppants and acids may be considered as well. The ultimate goal is to make production economically and maximize well performance (Beaman & McNeil, 2012). Fracturing can be used to bypass near-wellbore damage and to alter fluid flow in the formation, as well (Economides & Nolte, 2000). Fracturing technologies have been applied for more than 60 years. Only few important latest and widely used technologies will be explained in this Chapter.

Fracture pattern at a rock during stimulation can alter due to reservoir and well-design parameters. Permeability along with local stress regime (especially the minimum principal stress - σ_3) are more decisive among other reservoir parameters (Economides & Nolte, 2000). The minimum principal stress as a pre-indicator of a fracture direction during hydraulic fracturing has a great importance. As it is postulated, a fracture plane would most likely occur normal to the direction of a minimum principal stress (Hubbert & Willis, 1957). Well-design parameters for fracturing determines fracture pattern with reservoir parameters. Some basic steps and factors are required to design a well wherein fracturing will be performed. Those controlling factors during a fracturing treatment planning at a reservoir are summarized below and depicted as a flow schema in the Figure 21.

In order to determine wellbore location and orientation before fracturing, it is recommended to find firstly sweet spots where dense clumping of a source is observed in a rock mass. Then the well drilling - casing - completion designs and fracture placement design, which depends on above mentioned factors (see also Figure 21), should be determined before the on-site treatment will be conducted. According to Ramakrishnan et al. (2011) the sweet spots can be defined by combining reservoir quality (e. g. effective porosity, permeability) and completion quality (e. g. type of fracture geometry obtained for a given stimulation treatment). However, for ore extraction applications, another factor for the definition of sweet spots emerges and that is the existence and location of natural fractures (Kennedy et al., 2012).

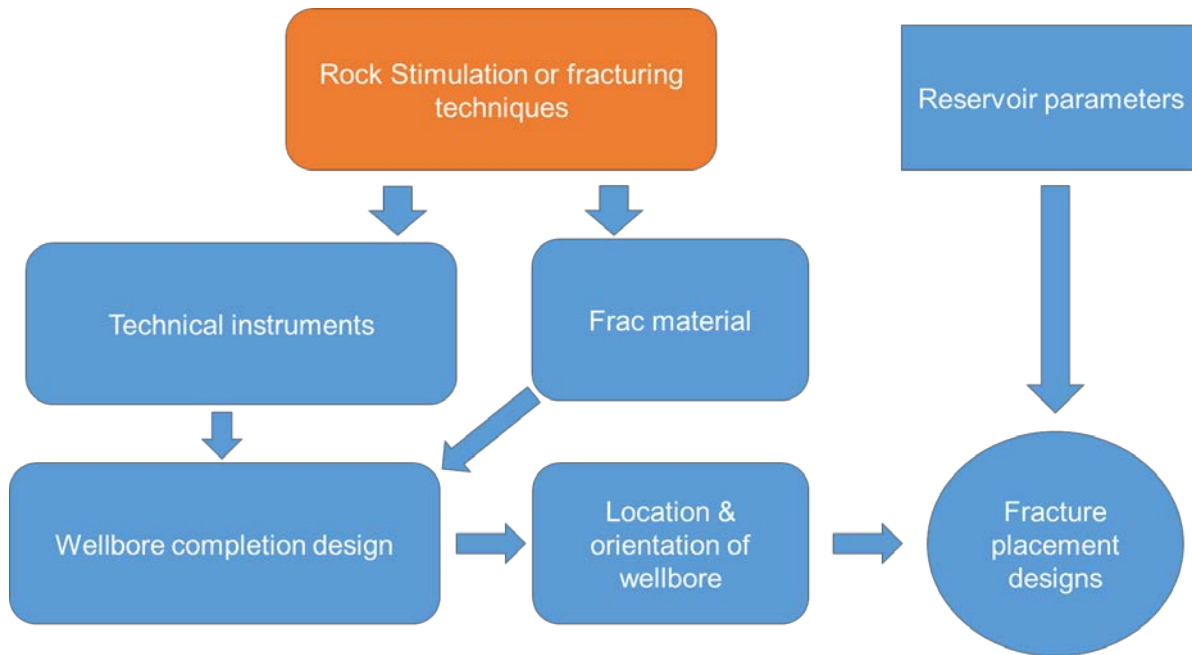


Figure 21 Simplified flow scheme defining the interdependency between the factors of rock stimulation which influence fracture placement designs together with reservoir parameters.

2.1 Technical instruments and fracking materials

Important technical instruments used during and after the rock stimulation are: annular isolators (e. g. straddle packers), mechanical isolators (e. g. shift or sliding sleeves, ball sealers and ball seat systems), plugs, pipes, coiled tubing and perforation tools. It should be noticed, that fracturing applications by using “coiled tubing” have been mostly preferred. Coiled tubing is a ductile steel tubing (or conduit) with small diameters (usually 1” to 1-3/4”), which is coiled onto a reel and can be used for pumping fluids (also cement) into the wellbore (API 1993). Keshavarzi (2011) defined a perforation as a process of creating tunnels through the cemented steel casing and rock formation to let the formation fluid flow into the well. This definition is valid for applications in petroleum industry and perforation can be conducted along uncemented parts of a wellbore, too.

Diverse fracturing materials are summarized in Table 1. It should be noted that when a gas is used as a fracturing material then this treatment is not usually defined as the „hydraulic fracturing”. The term “hydraulic fracturing” is mostly given to a stimulation treatment at which a liquid is used, for instance water, acid or oil.

Table 1 Fracturing materials used during a stimulation.

Fluid type	water, acid, foam, gel, high brine tolerant polymer, (liquid) resin, nitrogen, polysaccharide fracturing fluids, propane (LPG), propellant, (supercritical) CO ₂ , viscous oil and etc.
Others	Chemical additives, explosives, proppants, surfactants
Hybrid fluid	Slickwater ¹ together with proppant, and etc.

Note: ¹It is composed primarily of water and sand.

In case of considering only hydraulic fracturing, used fluid can be then divided into three main components (Xiong et al., 1996; Gandossi, 2013):

Fracturing Fluid = Base Fluid + Additive + Proppant

The common base fluids are water-based, foam-based, oil-based, acid-based, alcohol-based, emulsion-based and other fluids (liquid gases). Chemical additives are used to retard the growth of scale and bacteria around the wellbore, and it also serves for lowering viscosity of base fluid (e. g. Methanol and Liquid CO₂). In order to prevent the closure of created fractures after the fracturing treatment at a rock, it is necessary to introduce some type of particles called propping agents or proppants to hold the faces of fracture apart and afford a highly permeable conductive channel from the formation to the well (Donaldson, Waqi, & Nasrin, 2013). These can be any natural or synthetic material such as well-sorted sand, glass beads, walnut hulls and other types of synthetic particles.

According to Gooma et al. (2014), created fracture complexity has a strong relation with the fracture fluid type as viscosity and acidity plays an important role. Reducing the viscosity and/or increasing the acidity of the fluid may increase fracture complexity. Moreover, he concluded that Nitrogen gases will maximize the fracture complexity. This is shown in Figure 22. The least and most fracture complexity might be obtained by using crosslinked gel (very high viscosity) fluids and gases, respectively.

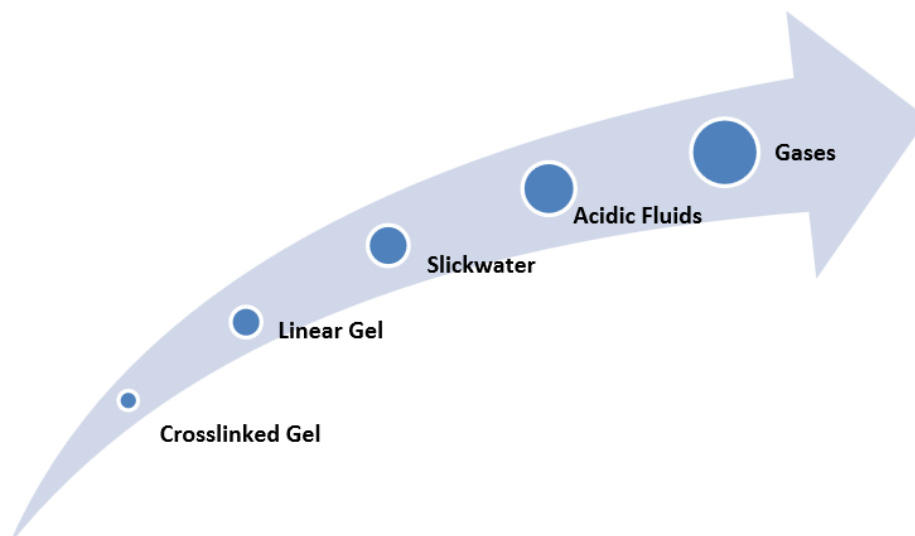


Figure 22 Correlation between used material for stimulation and fracture complexity (Gooma et al., 2014)

A comparative illustration of influence of fracturing material on fracture pattern (Fig. 25) is given by Safari et al. (2013). By using hydraulic fracturing (a) one single fracture aligned with the direction normal to the minimum principal stress can be generated. However, by using explosive (b) and pulsed gas (c) the fracture pattern can be more complex, which is consistent with Figure 22. Radial fractures may occur which seems to be preferential, nevertheless, this may trigger uncontrolled fracture growth and seismic events due to the complex behaviour of gas and destructions by explosives, respectively.

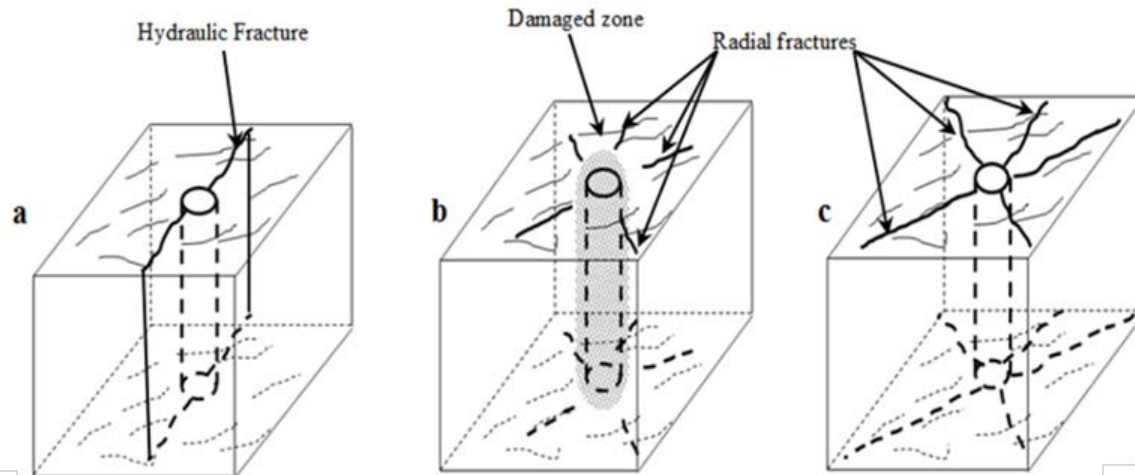


Figure 23 Fracture patterns from various techniques; Hydraulic (a), explosive (b) and pulsed gas (c) fracturing (Safari, et al., 2013).

Advantages and disadvantages together with applicability of most recent fracturing fluids and techniques applied for shale gas production are summarized under chosen key factors in Table 2. Fracturing techniques are classified under three categories as: dynamic, hydraulic, pneumatic and other. This concept is adapted from Gandossi (2013). At this table the symbols plus (+) and minus (-) for a fracturing fluid or technique stands for advantage and disadvantage under regarding key factor, respectively. For instance, using a thermal fracturing technique, which is classified under the other, will exhibit one advantageous and two disadvantageous features during an on-site operation (a key factor). According to this table, the frac-fluid LPG seems to be a convenient fracturing fluid since it exhibits nine advantageous and only two disadvantageous features. Although applicability of this method is indicated as not available by the author, some studies considering LPG based fracturing performed at shales have been found (see Soni 2014 and Leblanc et al. 2011). Unlike frac-fluid LPG, electric fracturing technique exhibits two advantageous and three disadvantageous features and its applicability for shales is indicated as under development, so that this technique may be considered as inconvenient.

Hydraulic fracturing

Only for private and internal use!

Updated: 18 March 2022

Table 2 Qualitative comparison for fracturing fluids and fracturing techniques applied for shale gas production (adapted from Gandossi 2013).

FRAC-FLUIDS OR FRAC TECHNIQUE (Type)	KEY FACTORS						
	Fluid usage	Environmental impact	On-site operation (before & after)	Reservoir productivity	Reservoir integrity	Costs	Applicability for shale
Foam-based (H)	+	++	+ -	-	-	-	Yes
Oil-based (LPG) (H)	+	++ -	+++	+++	-	-	NA
Acid-based (H)	NA	NA	NA	NA	NA	NA	NA
Alcohol-based (H)	+	+ -		+			NA
Emulsion-based (H)	+	+		+		-	NA
Liquid CO ₂ (H)	+	++	++ -	+ -	-	-	Yes
Liquid N ₂ (H)	+	++	-		+	-	Yes
Liquid He (H)	+	++	-	-		-	Yes
Liquid LPG (H)	NA	NA	NA	NA	NA	NA	Yes
Air, N ₂ (P)	+	+	-	-	+		Yes
Explosive (D)	+	+ -	+	+++ -	+	+	Yes
Electric fracturing (D)	+	+		- - -			UD
Thermal fracturing (O)	+	++	+ - -				UD
Mechanical cutting (O)	+	+	+	+			UD
Enhanced bacterial methanogenesis (O)	+	+		+			UD
Heating of the rock mass (O)	+	+					UD

Fracturing types	Notation
Hydraulic	H
Pneumatic	P
Dynamic	D
Other	O

Note: "NA" stands for "information not available", "UD" stands for "under development"

2.2 Wellbore completion design

One of the criteria to classify the wellbore completion types is the fracturing stages and instruments used during the treatment. The fracturing stage indicates a location at the wellbore where a fracturing treatment is performed. It can be one location during an intended time interval, then it is called “single-stage fracturing” or it can be more than one location then it is called “multistage or multi zone fracturing”.

There are several multistage fracturing treatments, however only three most effective and efficient methods used in American shale plays for gas/oil production will be examined in this chapter. These are coiled-tubing-activated, plug-and-perforate and ball-activated systems (Beaman et al. 2012, Kennedy et al. 2012 and Yuan et al. 2013). The SWOT (Strength-Weakness-Opportunity-Threat) analysis of those most common used wellbore completion systems is given in Table 3.

Coiled tubing fracturing method mainly relies on the “Bottom Hole Assembly (BHA)” concept. The BHA concept mentioned here is a combination of packers and perforation tools integrated on a coiled tubing (see Figure 24). Packer has the function of zonal isolation between perforated intervals and a perforations-tool is used to perforate along the intended stage before the stimulation will be conducted by selected fracking material. Clean up of any residual after a fracturing procedure can be also performed within a coiled tubing work string at a wellbore annulus. Instead of packers, other instruments such as casing sleeves and hydrjets (on coiled tubing) can be used, as well. The one of a popular coiled tubing fracturing method using hydrjets is called “pinpoint fracturing” (for more information see Lopez-Bonetti et al. 2014).

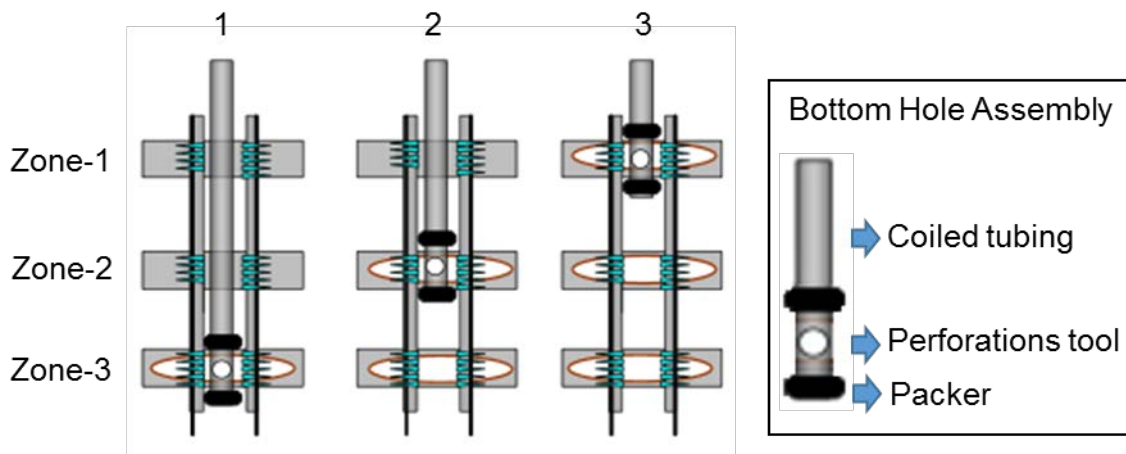


Figure 24 Sequential illustration of coiled tubing fracturing procedure (adapted from Gulrajani et al., 1999).

The basic fracture procedure (from step 1 to 3) by coiled tubing is depicted in Figure 4. It should be noticed that all zones were perforated (shown by blue triangles) before the stimulation has been initiated. The BHA is driven into the bottom of a wellbore against an intended zone to create fractures. Straddle packers are blown up to ensure the isolation during a fracture treatment. If required then clean-up will be performed upon completion of a fracture treatment while BHA pulling up to a next zone by loosening packers. The procedure (isolation, fracturing, clean-up) will be started from the beginning for other intervals.

Plug-and-perforate fracturing is performed by moving coiled tubing through different stages at a well lateral. It is performed by using a perforations tool integrated on a coiled tubing and then injection of a selected fracturing material. At the end of an intended fracturing operation, plugs are removed by a milling head. A brief illustration of this method is depicted sequentially (from step 1 to 5) at the Figure 25. First of all, a plug is emplaced by using coiled tubing at the toe of a well lateral (step 1) and perforation is conducted along an intended stage (step 2). In order to perform fracturing operation, selected fracking material (here a fluid) is then injected through borehole casing (step 3). After completing the first fracturing procedure (emplacement of plugs, perforation and stimulation), same procedure will be started from the beginning for other stages along an intended interval from toe to heel of a well lateral (step 4). At the end of a planned fracture treatment, plugs are removed by using a milling head or a coiled tubing. Plugs have an important function that enable isolation in between these different stages where fractures were created by perforation and stimulation.

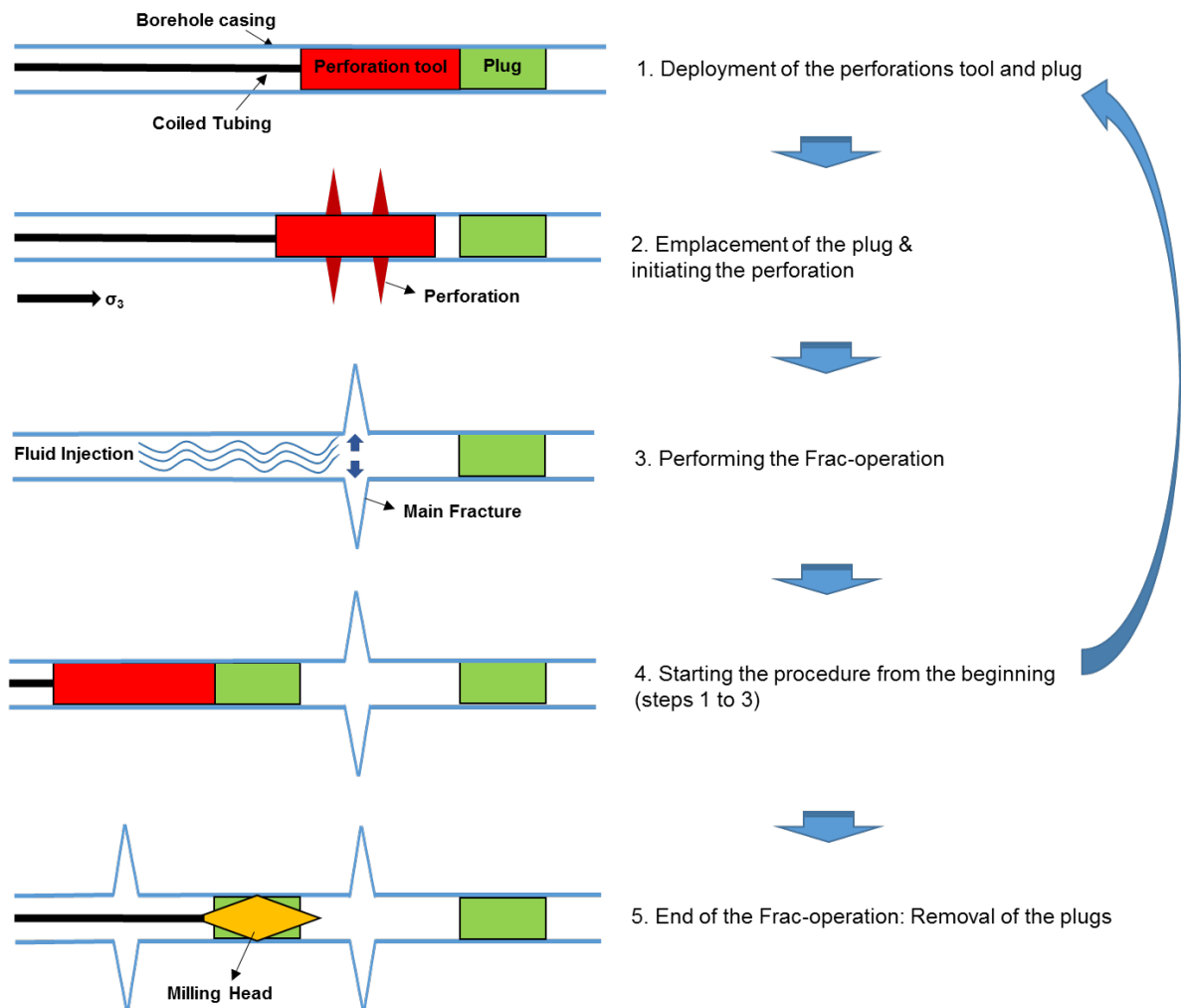


Figure 25 Sequential illustration of plug-and-perforate (plug-and-perf) fracturing procedure.

Ball-activated systems can be defined as a completion realised by dropping of graduated balls into sliding sleeves. It consists of three mechanical parts integrated on a liner hanger or on a long-string: Frac ports at where a fracking material is pumped; sliding sleeves which contains frac ports on it and shifts via pressure rise through the sealing of a dropped ball and opens frac ports; and finally gradually sized balls dropped from surface into sliding sleeves. Sliding sleeves shift and open frac ports along an

intended stage for fracturing. Frac ports can be then activated and fracturing can be conducted at intended operational depth by using the selected fracking material. Balls have a vital importance of offering both activation and sealing functions hence fracturing can be conducted through gradually sized balls at different stages. Figure 26 gives a brief sequential illustration (steps 1 to 5) of frac ports activation through seating of gradually sized balls in a wellbore.

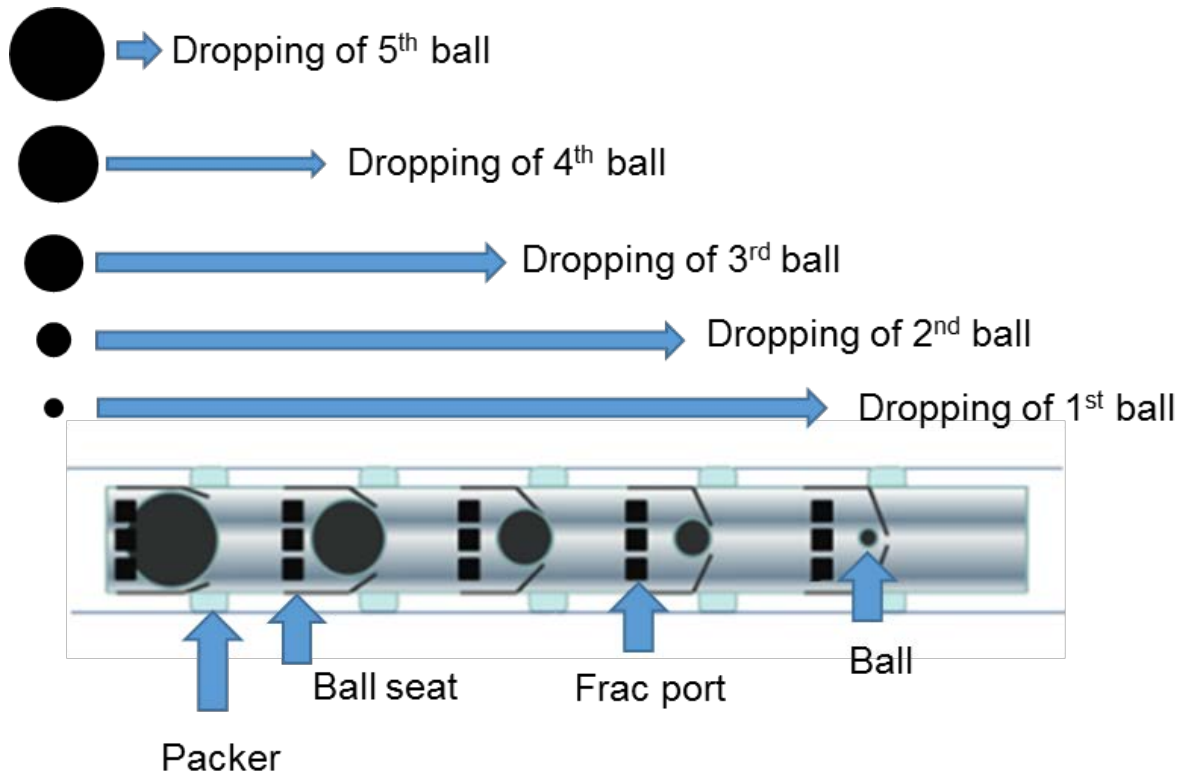


Figure 26 Sequential illustration of ball-activated fracturing procedure (adapted from Daneshy, 2011).

Table 3a SWOT analyses of three common wellbore completion systems: Coiled-Tubing system (Daneshy, 2011; Gulrajani & Olmstead, 1999; Kennedy *et al.* 2012; Lindsay *et al.* 2012; Moslavac *et al.* 2010; Thomson, 2014)

Coiled-Tubing system:		Positive	Negative
Internal	S trength:	<ul style="list-style-type: none"> - Most accurate fluid placement into each stage during shut-downs - Coiled tubing readily available for premature screen outs* - Efficient fracture treatment - Accelerated production 	W eakness: <ul style="list-style-type: none"> - Lower injection rates - Available <i>weight on bit</i> at depth for setting tools – causes depth limitations
	O pportunities:	<ul style="list-style-type: none"> - Reduced maintenance and logistical issues - Less fluids required - Perforating, fracturing and diversion in a single trip - Less chance of over-flushing near wellbore 	T hreads: <ul style="list-style-type: none"> - Higher surface pressures required due to increased frictional pressure losses - Slower than sliding sleeves - Increased pump time versus plug & perf method
External			

Note: * Interference occurred at flow area due to transported solids (e. g. Proppant) in a fluid used for stimulation.

Table 4b SWOT analyses of three common wellbore completion systems: Plug & Perforate system (Daneshy, 2011; Gulrajani & Olmstead, 1999; Kennedy *et al.* 2012; Lindsay *et al.* 2012; Moslavac *et al.* 2010; Thomson, 2014)

Plug-and-perforate system:	Positive	Negative
Internal	<p>Strength:</p> <ul style="list-style-type: none"> - Considered reliable and efficient - Best overall recoveries - With micro-seismic fracture mapping can avoid geo-hazards or need of offset wells - Full bore after plug mill out 	<p>Weakness:</p> <ul style="list-style-type: none"> - Multiple trips into well - Depending on number of stages, this technique can take several days or more
External	<p>Opportunities:</p> <ul style="list-style-type: none"> - Best placement of fractures - Flexibility: Treating individual stages and changing design at the same time - Advanced fracturing techniques 	<p>Threads:</p> <ul style="list-style-type: none"> - Has higher intervention costs when compared to other techniques such as sleeves - High amount of over-flushing – reduced fracture conductivity

Table 5c SWOT analyses of three common wellbore completion systems: Ball-Activated systems (Daneshy, 2011; Gulrajani & Olmstead, 1999; Kennedy *et al.* 2012; Lindsay *et al.* 2012; Moslavac *et al.* 2010; Thomson, 2014)

Ball-activated systems:	Positive	Negative
Internal	<p>Strength:</p> <ul style="list-style-type: none"> - More efficient – reduced field operating time (allows for wells to come on production faster than does the plug-and-perforate method) - Less frequent screen out - Several stages can be stimulated in a single day 	<p>Weakness:</p> <ul style="list-style-type: none"> - Less control on fracture location and number - Difficulty to re-fracture - Harder to clean out in case of premature screen out-drill out baffles (plates)

External	O pportunities: <ul style="list-style-type: none"> - Reduced cost due to field operation time - Reduced amount of over-flushing required compared to the plug & perf method - Simpler from a logistical point of view (e. g. no need of composite plugs and perforation-tools) 	T hreads: <ul style="list-style-type: none"> - Possible tool mal-functions and unless milled loss of full bore - Risk of poor isolation due to enlarged boreholes or wash outs - In-flexible: Changes cannot be made in stage depths
-----------------	--	--

One of a promising cutting-edge technologies is the laser perforation as a non-explosive alternative for hydraulic fracturing in oil and gas wells (Keshavarzi 2011, Batarseh et al. 2005). Different types such as fibre laser are available. Schematic illustration of a wellbore with laser perforation and observed fractures around the lased hole are shown in Figure 27. Many benefits of using laser technology at limestone, sandstone and shale were reported by Batarseh et al. (2012) and Keshavarzi (2011). Those are:

- Precision of controlling hole dimensions and orientation,
- Improvement of porosity and permeability which may result in the higher rate of production,
- Non-explosive and non-damage application, facilitate the fracture propagation by using thermal energy,
- Control of rock phase (spalling, vaporization, melting) by adjusting the laser power,
- Initiation of macro and micro fractures at a rock.

Moreover, Batarseh (2001) reported that up to 28 % permeability increase was reached by comparing lased with non-lased shale samples by using high power laser at the laboratory. Although this increase is not significant comparing to the one in the shaly sandstone (171 %), this laser application has no limitation in penetrating these rocks unlike conventional penetration methods as the author emphasized. Bakhtbidar *et al.* (2011) reported that, by using pulsed CO₂ laser beam the permeability of the rock increases up to 566 % compared to non-lased rocks. The laser technology is expected to facilitate hydraulic fracturing treatments in future. Nevertheless, probable disadvantages of using lasers due to thermal impact on rock remain to be more investigated. Some issues regarding losing energy in transmitting power to deep and controlling subsurface pressure are pending (Adeniji 2014).

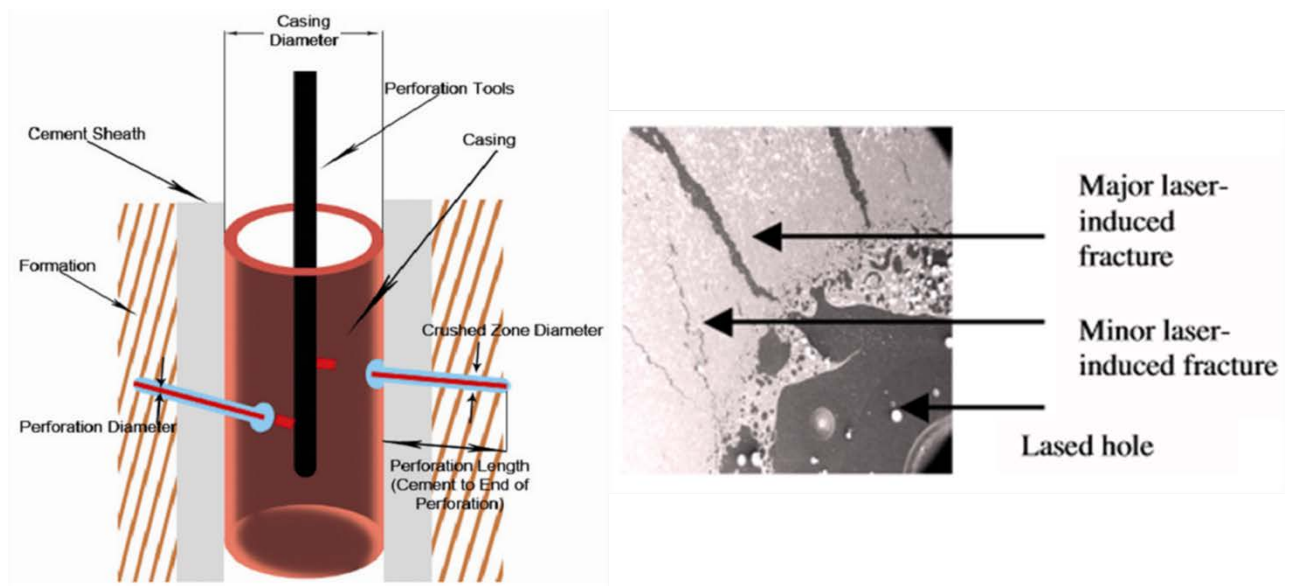


Figure 27 Schematic illustration of laser perforated wellbore (Bakhtbidar *et al.* 2011, left figure) and SEM (Scanning Electron Microscope) image of near-hole laser induced micro and macro fractures at shale (Graves and Bailo 2005, right figure).

2.3 Location and orientation of wellbore

Location, orientation and number of wellbores used for fracturing plays an important role before designing a fracture placement. In order to perform a fracturing operation in a reservoir, mostly vertical wellbores have been used and designed to produce from a single production string. Other types are given below (Economides & Nolte, 2000):

- Deviated wells: They are commonly drilled from fixed drilling locations and the drill bit is deflected at an angle from the vertical toward a specific target (Shepherd, 2009).
- Horizontal wells: The reservoir section is drilled at a high angle by horizontal wells, typically with a trajectory to keep the well within a specific reservoir or hydrocarbon zone (Shepherd, 2009).
- Multiple laterals or multilateral: They are wells that have more than one branch radiating from the main borehole. Each branch can drain a separate part of the reservoir and produce into a common single wellbore (Shepherd, 2009).
- Multiple completions: Oil well in which there is production from more than one oil-bearing zone (different depths) with parallel tubing strings within a single wellbore casing string (Parker & Licker 2002). Permanent completion tools (e. g. perforating plugs, retrievable plugs) and packers are typical instruments employed for multiple completions (Althouse & Fischer 1958).

Some wellbore types drilled through a target formation (red lines) and created fractures at multiple stages are depicted in Figure 28. It should be noted that directional wellbore at this Figure is a combination of vertical and deviated wellbores. A conceptual wellbore trajectory and anticipated fractures created along a wellbore are given at the same Figure as well. From a conventional mechanical point of view, direction of main fracture planes is estimated to follow the direction normal to the minimum principal stress (σ_3). Before initiating a fracture placement design, orientation of a wellbore trajectory should

be thus planned in accordance with the minimum principal stress direction. Furthermore, the recommended key factors for shale well-completion designs were given by Chong *et al.* (2010), these are:

- Fracability: Capability of the reservoir to be fracture-stimulated effectively,
- Producibility: Capability of the completion plan to sustain commercial production,
- Sustainability: Capability of the field development to meet both economic and environmental constraints.

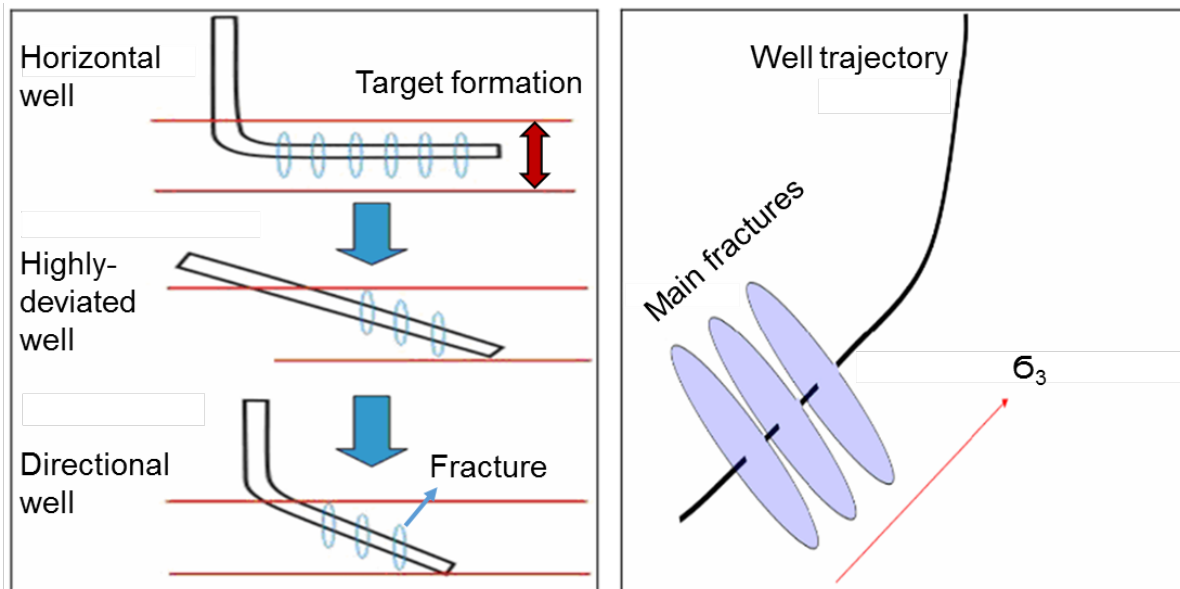


Figure 28 Different wellbore types used for multistage fracturing (left side) and conceptual well trajectory with predicted fractures on it (right side) (Chang, et al., 2013).

2.4 Fracture placement design

After selecting most convenient well completion design and fracturing material and also determining location, number and orientation of wellbores, fracture placement design can be then realised. Widely used fracture placement designs employing multistage fracturing techniques are summarized into two groups which are: zipper and alternating fracturing. Zipper fracturing is divided into 3 categories:

- Simultaneous zipper fracturing:

In order to enhance the stimulation of natural fractures in a rock, simultaneous fracturing at both parallel wellbores are conducted at the same time (shown with t_1 , see Figure 29, leftmost side). The fracturing mechanism relies on the induced stress near the tips which force propagation to direction normal to the main fracture in each cluster within the same time interval (Rafiee, Soliman, & Pirayesh, 2012). As Yu & Sepehrnoori (2013) stated, this fracturing concept is applicable to shale formations and slick-water is mainly used as a fracturing fluid.

- Sequential zipper fracturing:

Stages that are planned to be fractured are conducted sequentially (see Figure 29, middle), which means that it will be started to fracture the first stage (shown with t_1) at the well-1 then it will be continued with the second stage (shown with t_2) at the well-2 and so on. In this fracturing concept, it is anticipated to enhance the stimulation of natural fractures when well-2 is stimulated via changing the residual stress field from well-1 wherein stimulation was already initiated before (Nagel et al., 2013).

- **Modified-zipper fracturing:**

With this concept it is aimed to enhance the stimulation of natural fractures along off-setting stages of two wellbores. The same methodology is used like at sequential fracturing and only difference is that wells are horizontally shifted according to each other (see Figure 29, rightmost side).

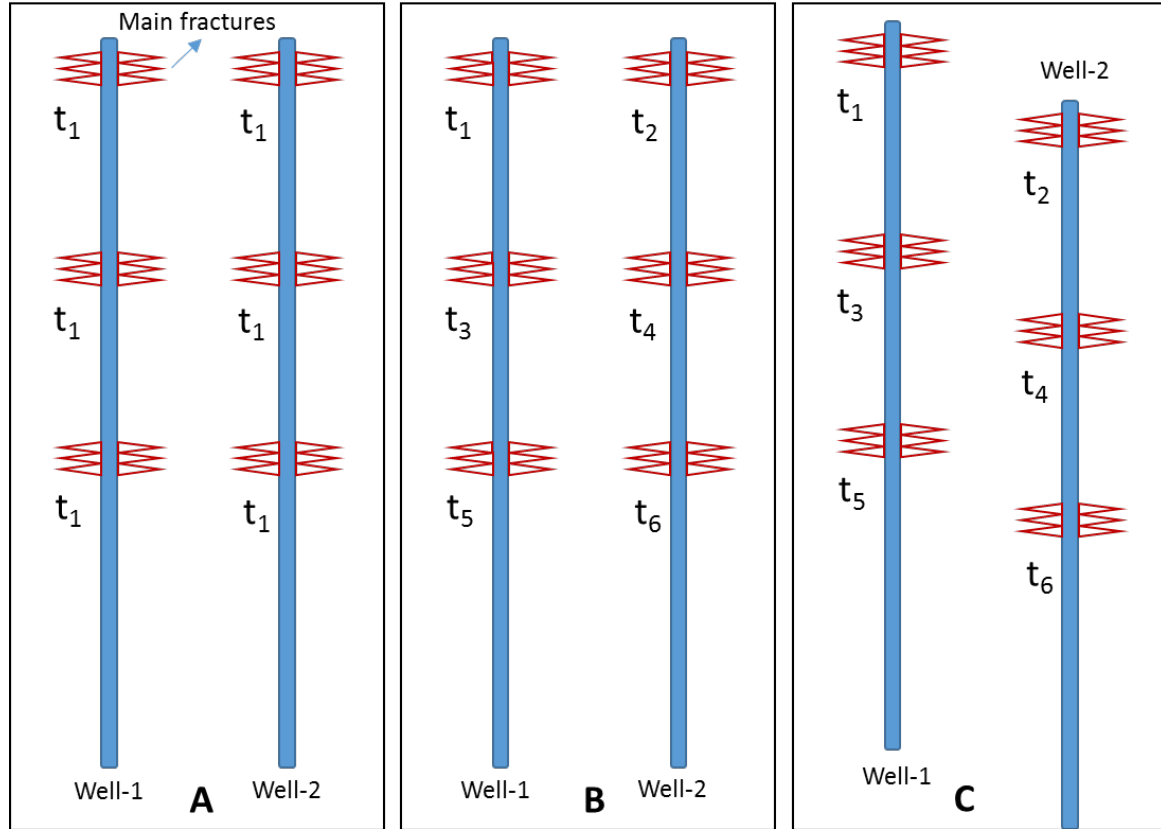


Figure 29 Simplified illustration of; Simultaneous (A), sequential (B) and modified (C) zipper fracturing concepts at parallel wellbores shown with time sequences per se (t_1 to t_6).

Except zipper fracturing concepts, there is one more widely used concept called “Alternating” or “Texas two – step” fracturing. Fractures are created in an irregular sequence of different stages at one wellbore. In Figure 30, numbers indicate these stage sequences where stimulation took place. As it is seen on that Figure, the stage with number 1 has been firstly stimulated, then the stage with number 2 and the stage with number 3, which is in between these two stages, were stimulated and so on. It is anticipated to obtain a complex network of fractures connected to main hydraulic fractures by altering the stress within the area between pre-stimulated stages and thus triggering the stress-relieved fractures (Rafiee, Soliman, & Pirayesh, 2012).

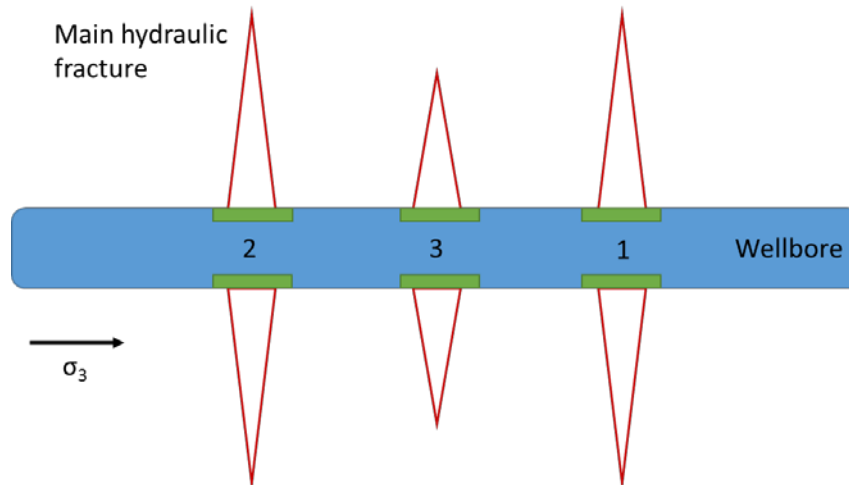


Figure 30 Simplified illustration of an alternating fracturing at a single wellbore shown with irregular stage sequences (numbers).

The distance between stimulation locations (fracturing stages) affects the fracture placement design due to “stress shadow effect” as well as other factors. Stress shadow effect during the hydraulic fracturing in crystalline rocks is mentioned by Zeeb, Wolgast & Konietzky (2014) and Zeeb & Konietzky (2015). This is an alteration of the in-situ stresses, especially the change in the minimum principal stress during the stimulation. As they added, evaluation of field data and simulation results indicate that stress shadowing affects both fracture propagation and geometry. Zeeb & Konietzky (2015) explained this effect by using the numerical code 3DEC. As authors stated, increasing the distance between stages and changing the orientation of borehole (45° towards σ_3) along with enabling drainage at the model diminish stress shadow effect (see Figure-36). Deflection of fractures were hence prevented, so more convenient fracture geometries were obtained for further HDR (Hot Dry Rock) applications at the granite.

Moslavac et al. (2010) and Lindsay et al. (2012) stated that especially hydrojetting system is seen as a promising technique and a revolutionary game changer for the entire fracturing industry.

Fracture data set among others is a key factor to develop an accurate fracturing placement design due to the possible presence of natural fractures at the rock. Log data, drilling cuttings and diagrams may be useful to assess modelling parameters. Auxiliary technologies, for instance geophysical subsurface methods, are strongly suggested to use in accordance with these modelling studies. Some of those are listed below:

- microseismic monitoring or mapping - also during hydraulic fracturing (e. g. Composite radiation patterns of micro-seismicity),
- wellbore real-time monitoring (e. g. Logging-while-drilling),
- natural fracture identification,
- geo-steering,
- magnetic resonance to identify permeability in shale reservoirs,
- acoustic characterization,
- mineralogy cuttings analysis,
- high resolution diffraction imaging of small scale fracture fields,
- high power laser application in open-hole multiple fracturing.

Figure 34 summarizes the elements of hydraulic fracturing design.

Drilling design (rotary steerable systems – RSS or laser drilling) and design of other wellbore completion elements such as tubing, liner, casing and conductor are not mentioned here. Subsequent to further drilling concept, wellbore trajectory should be designed in view of seismic, shale analyses and offset well data. Vertical and lateral variability in rock characteristics must be addressed to increase the potential of economic success as well (Miller, Waters, & Rylander, 2011).

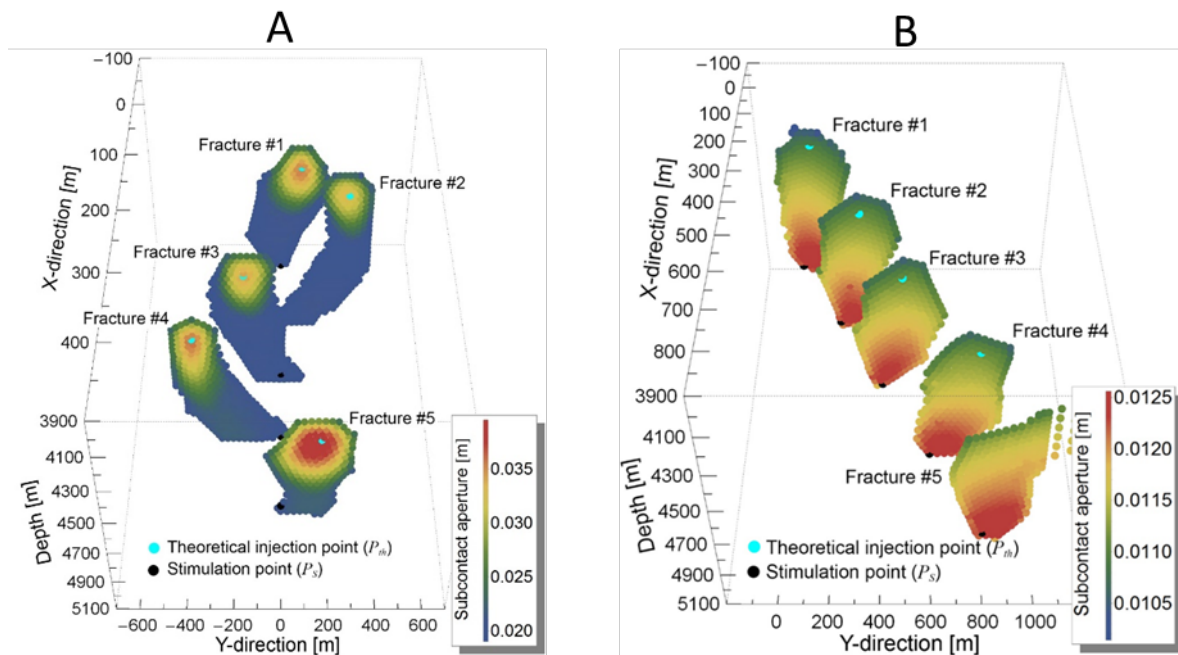


Figure 31 Simulation of multistage fracturing (A) influence of the stress shadow effect on fracture propagation, and (B) diminishing the stress shadow effect by changing the borehole orientation (Zeeb, Wolgast & Konietzky, 2014).

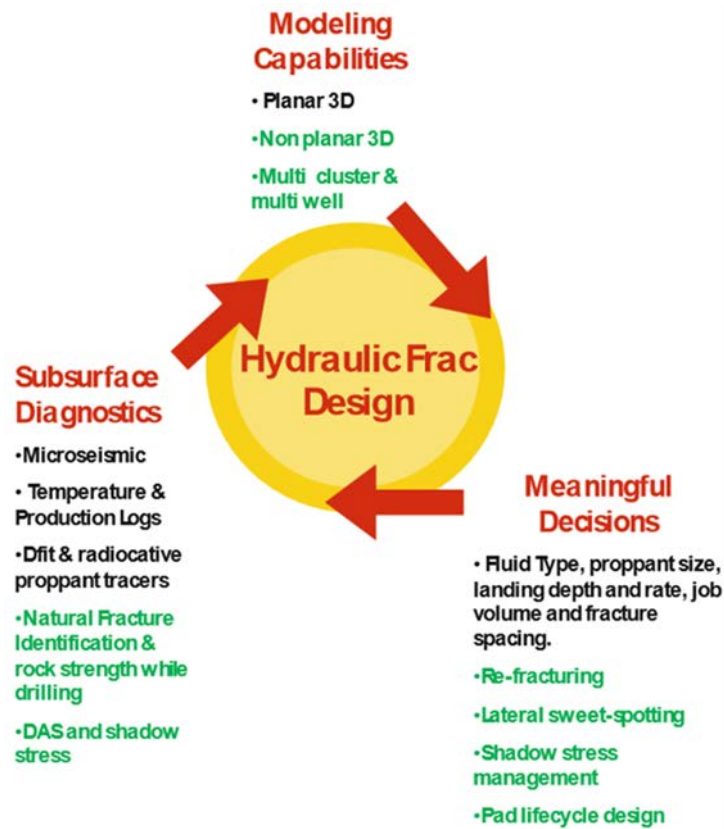


Figure 32 Schema of interaction between elements for hydraulic fracturing design (Fonseca, 2014). DAS stands for “Distributed Acoustic Sensing”.

3 Hydraulic fracture propagation in rock masses

Hydraulic fracture propagation in rock masses is influenced by many factors, a few of them are illustrated below via numerical simulations.

Figure 33 illustrates how two hydraulic driven fracture connect. Due to the stress shadow effect (caused by stress concentrations at the crack tips) the connection does not follow a straight line, but a curved route. The process can become even more complicated if heterogeneity and anisotropy in strength is significant.

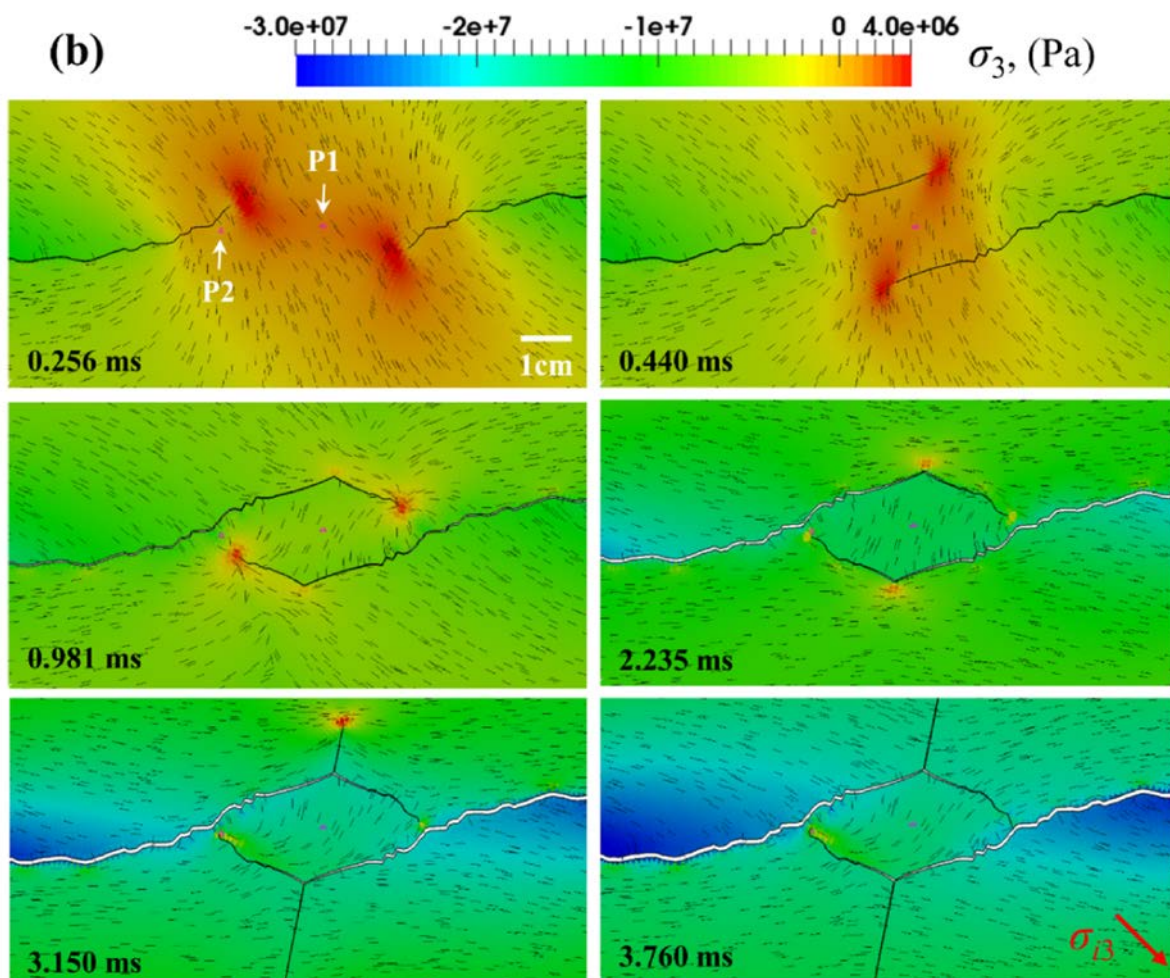


Figure 33 Directional hydraulic fracture propagation (principal stresses): intertwine of two hydraulic driven fractures (Bai et al., 2021)

Wasantha et al. (2019) investigated the influence of the stress contrasts in rock masses on the hydraulic fracture propagation, which is typically for layered sediments, for instance gas and oil reservoirs. Fig. 34 shows the general model set-up. Figures 35 and 36 illustrate how inhomogeneous stress field, stimulation sequence and distance between different fractures influence the fracture propagation.

Figure 37 documents that hydraulic fractures follow the initial orientation in homogeneous environment, but experience a reorientation (orientation parallel to maximum principle stress) in case of highly anisotropic stress fields.

Figures 38, 39 and 40 illustrate how natural fractures influence the propagation of hydraulic fractures. The considered constellations produce significant anisotropic fracture propagation (compare fracture wings).

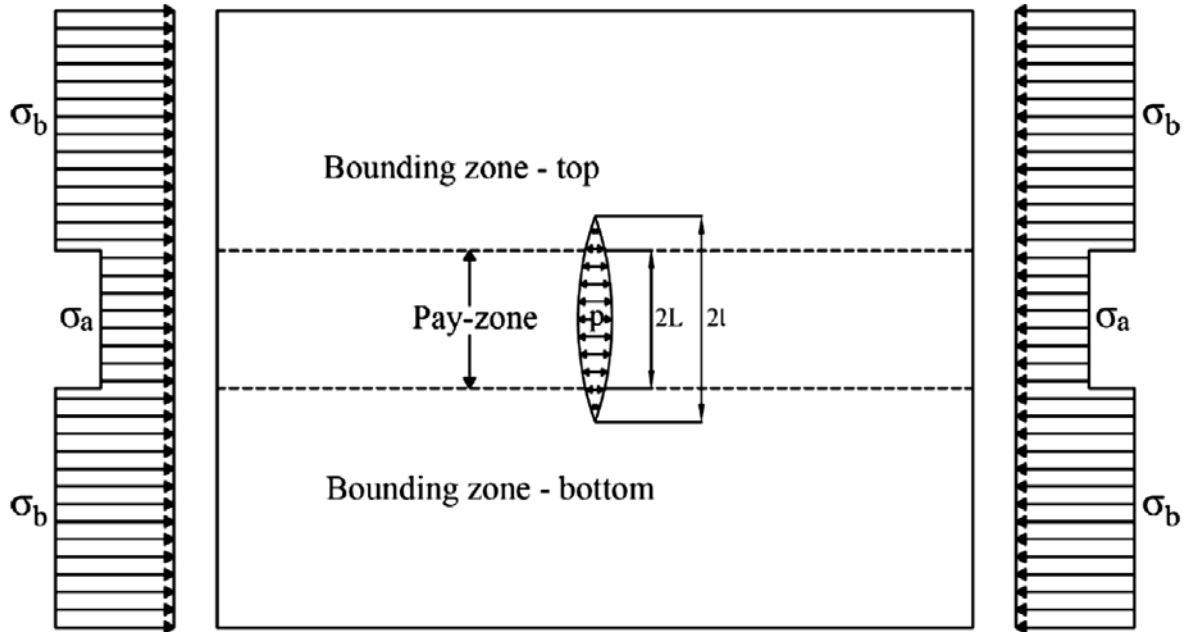


Figure 34 General model set-up to investigate single and multi-stage hydraulic fracturing considering stress inhomogeneity (Wasantha et al., 2019)

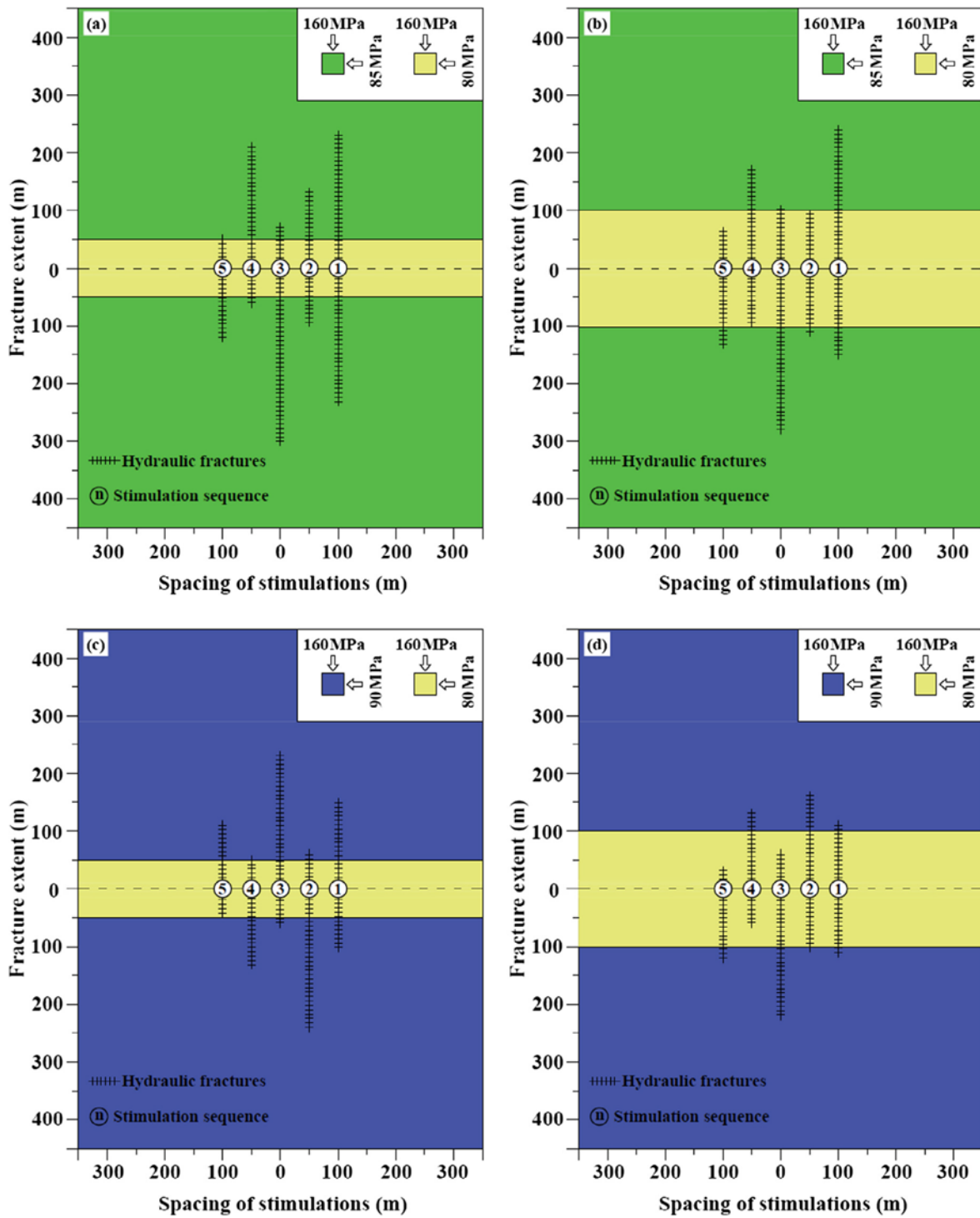


Figure 35 Hydraulic fracture profiles after 100 s of fluid injection, 50 m distance between fractures (Wasantha et al., 2019)

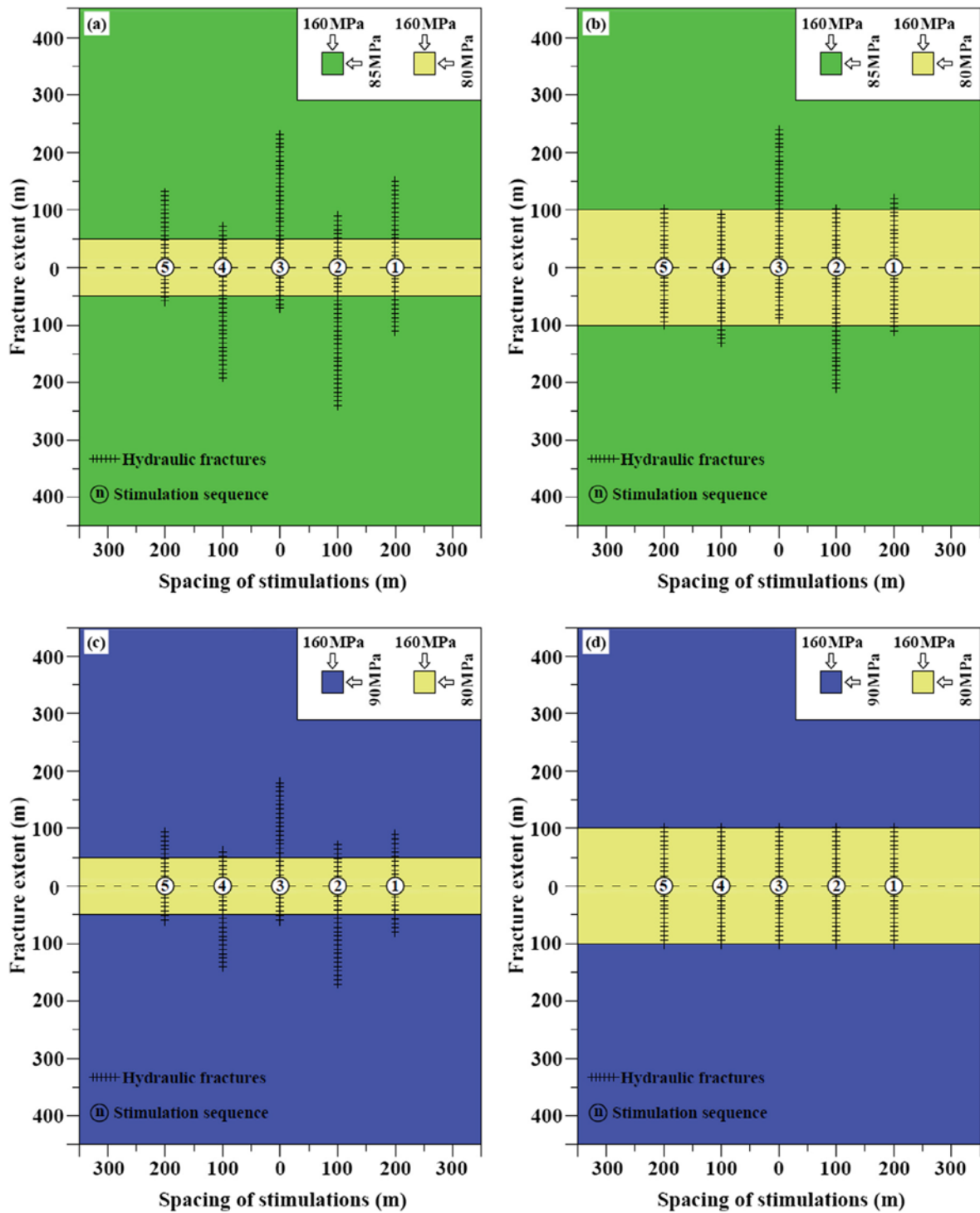


Figure 36 Hydraulic fracture profiles after 100 s of fluid injection, 100 m distance between fractures (Wasantha et al., 2019)

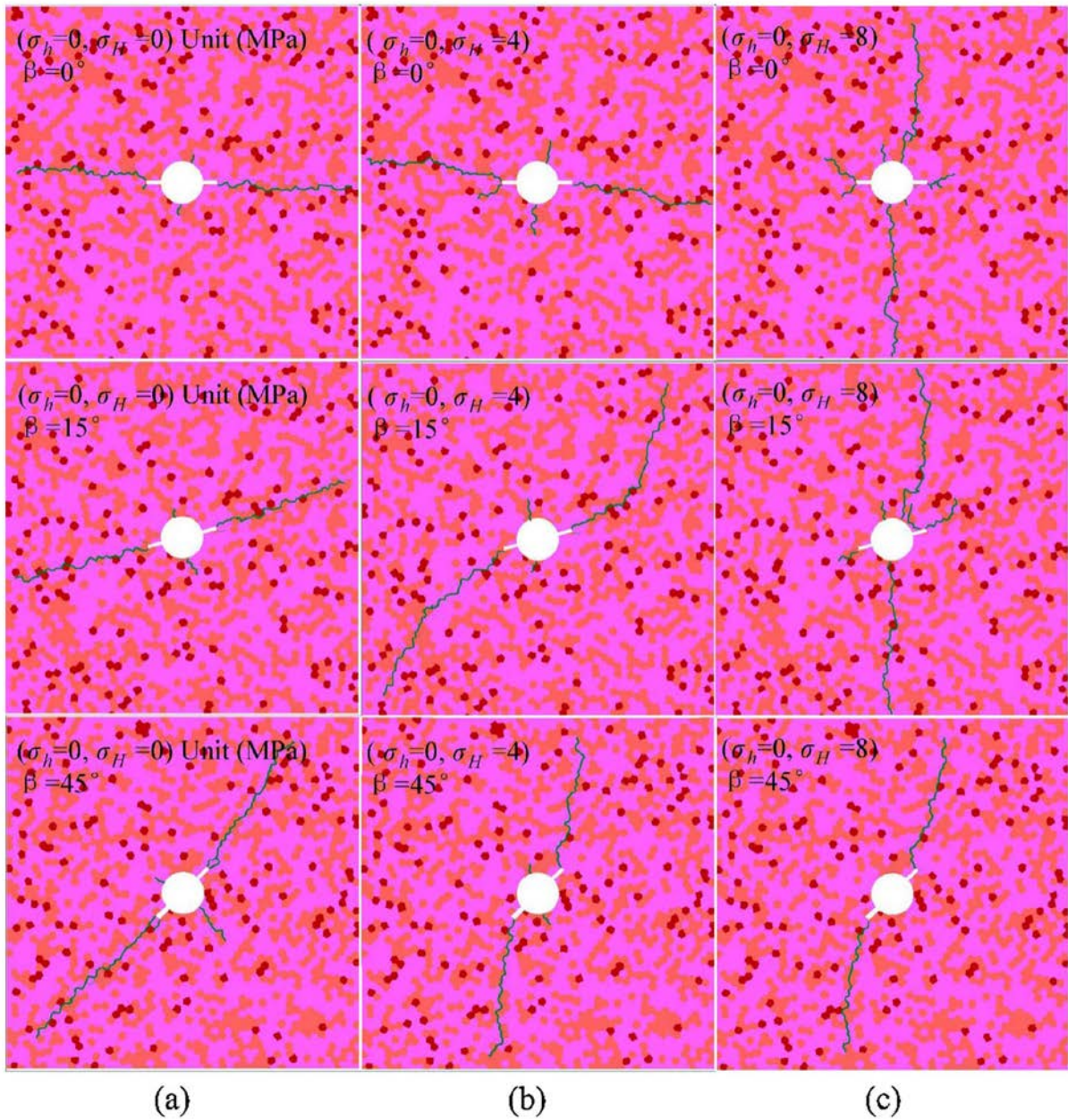


Figure 37 Hydraulic fracture patterns for different stress fields and pre-existing cracks (notches) of different orientation: (a) $\sigma_H = 0$ MPa, (b) $\sigma_H = 4$ MPa, (c) $\sigma_H = 8$ MPa, σ_h always zero (Chen et al., 2018)

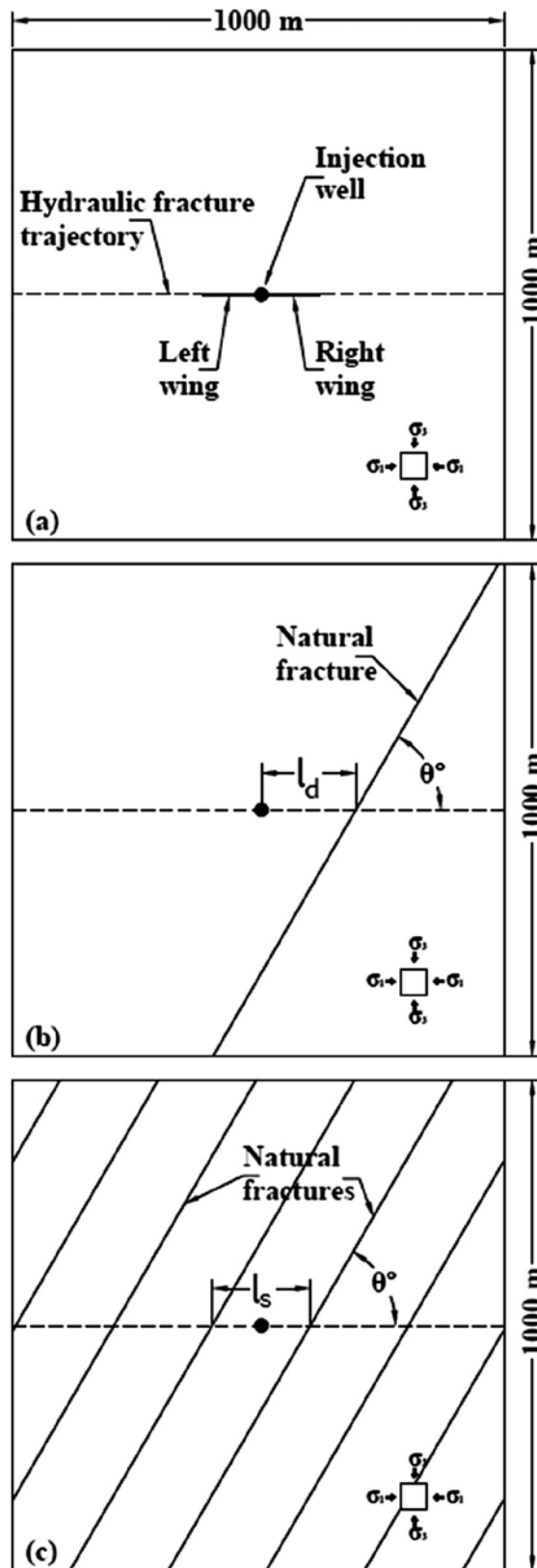


Figure 38 Numerical model set-up to investigate interaction of hydraulic driven fracture with natural fractures (Wasantha et al. 2017)

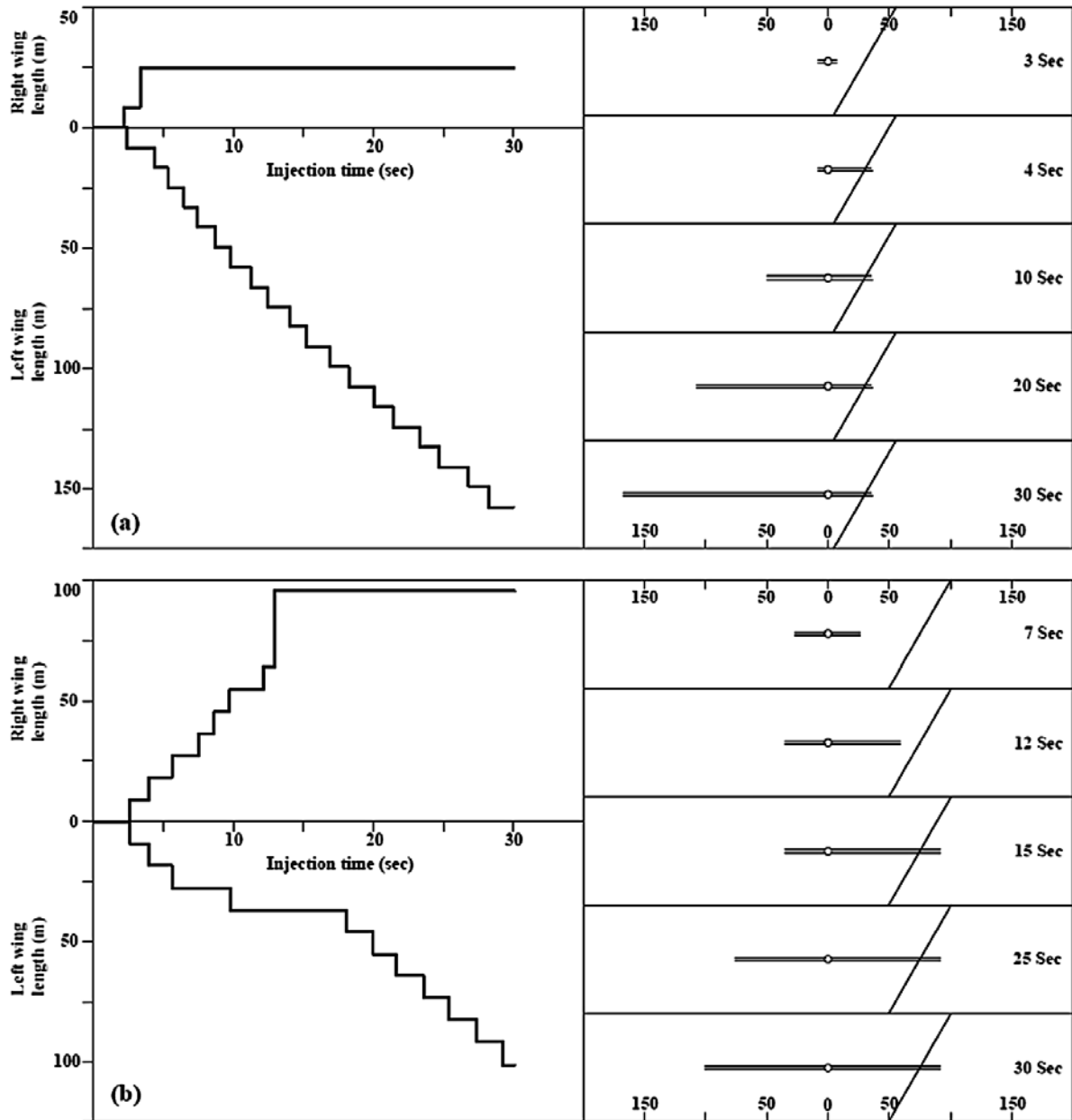


Figure 39 Fracture pattern for different constellations in respect to distance between injection point and single natural fracture (Wasantha et al. 2017)

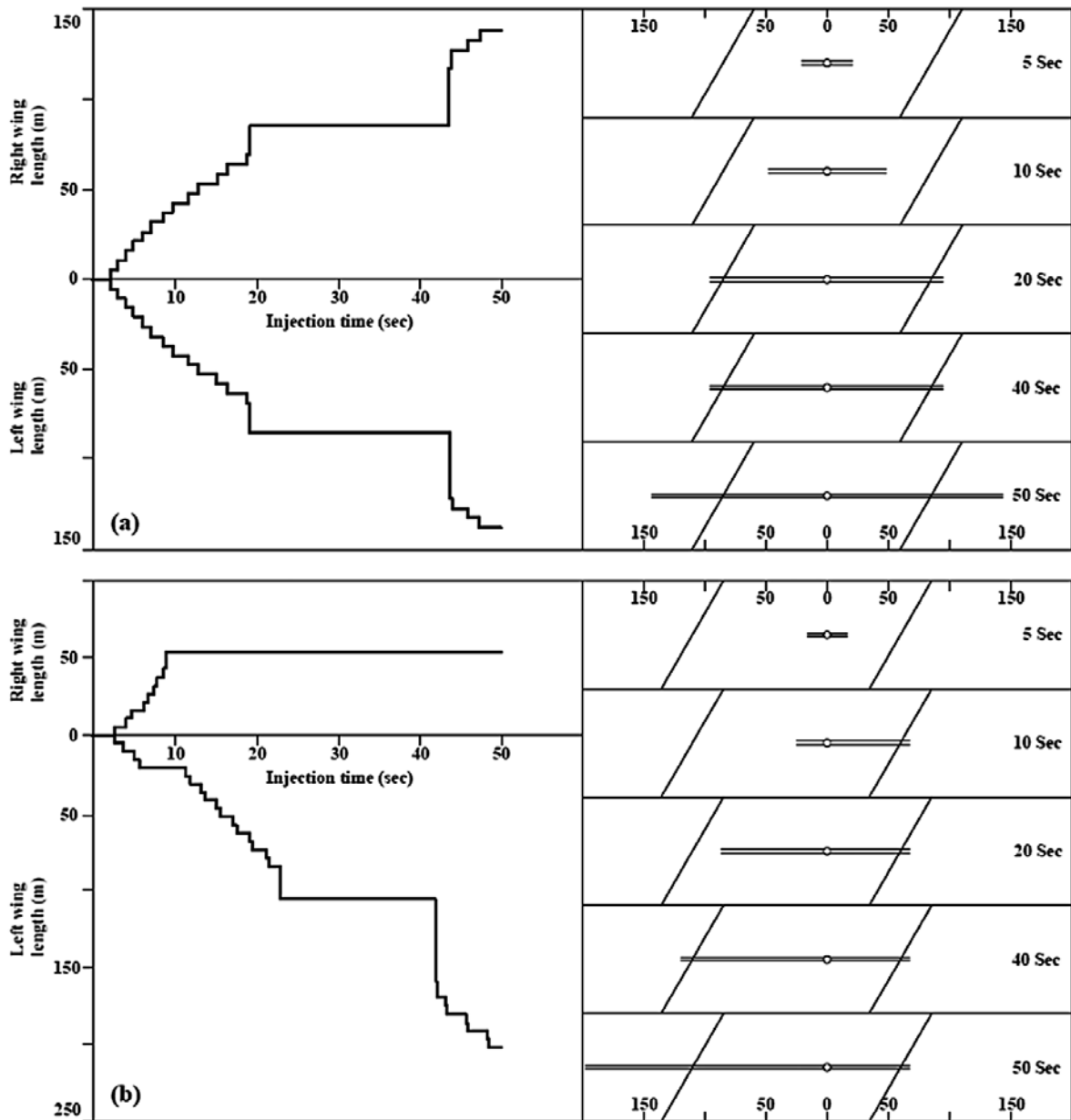


Figure 40 Fracture pattern for different constellations in respect to location of injection point between two natural fractures (Wasantha et al. 2017)

4 References

- Adachi, J. I., & Detournay, E. (2002). Self-Similar Solution of a Plane-Strain Fracture Driven by a Power-Law Fluid. *International Journal for Numerical and analytical Methods in Geomechanics*(26), pp. 579-604.
- Adachi, J., Siebrits, E., & Desroches, J. (2007). Computer Simulation of Hydraulic Fractures. *International Journal of Rock Mechanics & Mining Sciences* 44, pp. 739-757.
- Adeniji, A. W. (2014). The Applications of Laser Technology in Downhole Operations - A Review. Doha, Qatar: International Petroleum Technology Conference.
- Althouse W. S., Fisher H. H. (1958). The selection of a multiple completion hook-up. *Journal of Petroleum Technology*, 10(12).
- API. (2000). *Environmental Guidance Document: Well Abandonment and Inactive Well Practices for U.S. Exploration and Production Operations, Bulletin E3, First Edition*. USA: American Petroleum Institute.
- Bai, Q., Konietzky, H., Zhang, C., Xia, B. (2021). Directional hydraulic fracturing (DHF) using oriented perforations: The role of micro-crack heterogeneity, *Computers and Geotechnics*, 140: 104471
- Bakhtbidar, M., Ghorbankhani, M., Alimohammadi, M., Esfeh, M. R., & Rezaei, P. (2011). Application of Laser Technology for Oil and Gas Wells Perforation. Muscat, Oman: SPE/IADC Middle East Drilling Technology Conference and Exhibition.
- Barenblatt, G. I. (1961). The Mathematical Theory of Equilibrium Cracks Formed in Brittle Fractures. In *H. L. Dryden, T. von Karman (Eds.), Advances in Applied Mechanics, Vol. 7*. New York: Academic Press.
- Batarseh, S. (2001). *Application of Laser Technology in the Oil and Gas Industry: An Analysis of High Power Laser-Rock Interaction and its effect on Altering*, PhD Thesis. Colorado, USA: Colorado School of Mines.
- Beaman, D. J., & McNeil, F. (2012). New Hydraulic-Fracturing Process Enables a Low-Risk, Operationally Efficient Solution While Maximizing Stimulation Effectiveness in Unconventional Reservoirs. Abu Dhabi, UAE: Society of Petroleum Engineers, Middle East Unconventional Gas Conference and Exhibition.
- Brown, J. E., & Economides, M. J. (1992). Practical Consideration in Fracture Treatment Design,. In *Economides M. J.: Practical Companion to Reservoir Stimulation*. Amsterdam: Elsevier.
- Chang, Y., Lu, H., Chen, B., Ji, Z., Wang, C., Qi, Y., . . . Yin, G. (2013). Multi-Fracture Stimulation Techniques Make Better Wells in Ultra-Low Permeability Oil Reservoirs. Denver, Colorado, USA: Society of Petroleum Engineers, Unconventional Resources Technology Conference.
- Chen, W., Konietzky, H., Liu, C., Tan, X. (2018): Hydraulic fracturing simulation for heterogeneous granite by discrete element method, *Computers and Geotechnics*, 95: 1-15

- Chong, K. K., Jaripatke, O. A., Grieser, W. V., & Passman, A. (2010). A Completions Roadmap to Shale-Play Development: A Review of Successful Approaches toward Shale-Play Stimulation in the Last Two Decades. Beijing, China: Society of Petroleum Engineers, International Oil and Gas Conference and Exhibition in China.
- Daneshy, A. A. (2011). Hydraulic Fracturing of Horizontal Wells: Issues and Insights. The Woodlands, Texas, USA : Society of Petroleum Engineers, Hydraulic Fracturing Technology Conference.
- Detournay, E. (2004). Propagation Regimes of Fluid-Driven Fractures in Impermeable Rocks. *International Journal of Geomechanics*, pp. 35-45.
- Donaldson, E. C., Waqi, A., & Nasrin, B. (2013). *Hydraulic Fracturing Explained Evaluation, Implementation and Challenges* (1st ed.). Houston, Texas, USA: Gulf Publishing Company.
- Dvorkin, J., & Nur, A. (1993). Dynamic Poroelasticity: a Unified Model with the Squirt and the Biot Mechanism. *Geophysics*, pp. 524-533.
- Economides, M. J., & Nolte, K. G. (2000). *Reservoir Stimulation* (3rd ed.). New York, USA: John Wiley & Sons.
- Fjaer, E., Holt, R. M., Horsrud, P., Raaen, A. M., & Risnes, R. (2008). *Petroleum Related Rock Mechanics* (Second ed.). Amsterdam: Elsevier.
- Fonseca, E. (2014). Emerging Technologies and the Future of Hydraulic Fracturing Design in Unconventional Gas and Tight Oil. Doha, Qatar : International Petroleum Technology Conference.
- Gandossi, L. (2013). *An overview of hydraulic fracturing and other formation stimulation technologies for shale gas production*. Luxembourg: European Commission - Joint Research Centre, Institute for Energy and Transport.
- Geertsma, J., & de Klerk, F. (1969). A Rapid Method of Predicting Width and Extent of Hydraulically Induced Fractures. *Journal of Petroleum Technology*, pp. 1571-1581.
- Gomaa, A. M., Qu, Q., Maharidge, R., Nelson, S., & Reed, T. (2014). New Insights into Hydraulic Fracturing of Shale Formations. Doha, Qatar : International Petroleum Technology Conference.
- Gou, F., Morgenstern, N. R., & Scott, J. D. (1993). Interpretation of Hydraulic Fracturing Breakdown Pressure. *Int. J. Rock Mech. Min. Sci. & Geomech. Abstr.*, pp. 617-626.
- Graves, R. M., & Bailo, E. T. (2005). Analysis of Thermally Altered Rock Properties Using High-Power Laser Technology. Calgary, Alberta, Canada: Petroleum Society of Canada, Canadian International Petroleum Conference.
- Gulrajani, S., & Olmstead, C. C. (1999). Coiled Tubing Conveyed Fracture Treatments: Evolution, Methodology and Field Application. Charleston, West Virginia, USA: Society of Petroleum Engineers, Eastern Regional Conference and Exhibition.
- Hossain, M. M., Rahman, M. K., & Rahman, S. S. (2000). Hydraulic Fracture Initiation and Propagation: Roles of Wellbore Trajectory, Perforation and Stress Regimes. *Journal of Petroleum science and Engineering*, pp. 129-149.

- Hubbert, M. K., & Willis, D. G. (1957). Mechanics of Hydraulic Fracturing. *Transactions of Petroleum Engineers for the American Institute of Mining Engineers*, 210, 153-168.
- Itasca. (2013). *3DEC User's Guide, Version 5.0* (Fourth ed.). Minneapolis.
- Itasca. (2013). *FLAC3D User's Guide, Version 5.0.1* (Fifth ed.). Minneapolis.
- Iverson, W. P. (1995). Closure Stress Calculation in Anisotropic Formations. *SPE rocky mountain regional/low-permeability reservoirs conference*.
- Jing, L. (2003). A Review of Techniques, Advances and Outstanding Issues in Numerical Modelling for Rock Mechanics and Rock Engineering. *International Journal of Rock Mechanics & Mining Sciences*, 40, pp. 283-353.
- Kennedy, R. L., Gupta, R., Kotov, S. V., Burton, W. A., Knecht, W. N., & Ahmed, U. (2012). Optimized Shale Resource Development: Proper Placement of Wells and Hydraulic Fracture Stages. Abu Dhabi, UAE: Society of Petroleum Engineers, Abu Dhabi International Petroleum Conference and Exhibition.
- Keshavarzi, R. (2011). Laser Perforation for Hydraulic Fracturing in Oil and Gas Wells. San Francisco, USA: American Rock Mechanics Association, 45th US Rock Mechanics / Geomechanics Symposium.
- Kovalyshen, Y., & Detournay, E. (2010). A Reexamination of the Classical PKN Model of Hydraulic Fracturing. *Transport in Porous Media* 81, pp. 317-339.
- Leblanc, D. P., Martel, T., Graves, D. G., Tudor, E., & Lestz, R. (2011). Application of Propane (LPG) Based Hydraulic Fracturing in the McCully Gas Field. New Brunswick, Canada: Society of Petroleum Engineers, North American Unconventional Gas Conference and Exhibition.
- Lindsay, S. D., Ables, C., & Holden, D. R. (2012). Re-Innovating Old Technology Improves Efficiency of Proven Coiled-Tubing Stimulation. Port-of-Spain, Trinidad : Society of Petroleum Engineers, SPETT 2012 Energy Conference and Exhibition.
- Lopez-Bonetti, E., Araujo, O., Ortiz, J. R., Hernandez, J., Hazael, C., & Basurto, E. (2014). Improving Unconventional Completions by Pinpointing Multistage Fracturing With Coiled Tubing: Cases Histories from Burgos Basin. Maracaibo, Venezuela : Society of Petroleum Engineers, SPE Latin America and Caribbean Petroleum Engineering Conference.
- Miller, C. K., Waters, G. A., & Rylander, E. I. (2011). Evaluation of Production Log Data from Horizontal Wells Drilled in Organic Shales. The Woodlands, Texas, USA : Society of Petroleum Engineers, North American Unconventional Gas Conference and Exhibition,.
- Moslavac, B., Malnar, M., & Pasic, B. (2010). Multifracturing Well Completions. *The International Journal of Transport & Logistics*, 10(8).
- Nagel, N., Zhang, F., Sanchez-Nagel, M., & Lee, B. (2013). Quantitative Evaluation of Completion Techniques on Influencing Shale Fracture 'Complexity'. Brisbane, Australia : International Society for Rock Mechanics, International Conference for Effective and Sustainable Hydraulic Fracturing.
- Nordgren, R. P. (1972). Propagation of a Vertical Hydraulic Fracture. *Society of Petroleum Engineers Journal*, pp. 306-314.

- Parker, S. P., & Licker, M. D. (2002). *McGraw-Hill Dictionary of Scientific & Technical Terms* (6th ed.). New York, USA: The McGraw-Hill Companies, Inc.
- Perkins, T. K., & Kern, L. R. (1961). Widths of Hydraulic Fractures. *Journal of Petroleum Technology*, pp. 937-949.
- Rafiee, M., Soliman, M. Y., & Pirayesh, E. (2012). Hydraulic Fracturing Design and Optimization: A Modification to Zipper Frac. San Antonio, Texas, USA : Society of Petroleum Engineers, Annual Technical Conference and Exhibition.
- Ramakrishnan, H., Yuyan, R., & Belhadi, J. (2011). Real-Time Completion Optimization Of Multiple Laterals In Gas Shale Reservoirs: Integration of Geology, Log, Surface Seismic, and Microseismic Information. The Woodlands, Texas, USA: Society of Petroleum Engineers, Hydraulic Fracturing Technology Conference.
- Safari, R., Lakshminarayanan, S., Huang, J., Mutlu, O., Jayakumar, R., Christian, S. M., . . . Rai, R. (2013). Integrating Reservoir and Geomechanical Models to Compare the Productivity of Shale Reservoirs Using Different Fracture Techniques. Brisbane, Australia : Society of Petroleum Engineers, Unconventional Resources Conference and Exhibition-Asia Pacific.
- Saputelli, L., Lopez, C., Chacon, A., & Soliman, M. (2014). Design Optimization of Horizontal Wells With Multiple Hydraulic Fractures in the Bakken Shale. Vienna, Austria : SPE/EAGE European Unconventional Resources Conference and Exhibition.
- Savitski, A. A., & Detournay, E. (2002). Propagation of a Penny-Shaped Fluid-Driven Fracture in an Impermeable Rock: Asymptotic Solutions. *International Journal of Solids and Structures*, 39, pp. 6311-6337.
- Schmitt, D. R., & Zoback, M. D. (1989). Poroelastic Effects in the Determination of the Maximum Horizontal Principal Stress in Hydraulic Fracturing Test - a Proposed Breakdown Equation Employing a Modified Effective Stress Relation for Tensile Failure. *J. Rock Mech. Min. Sci. & Geomech. Abstr.* 26, pp. 499-506.
- Shepherd, M. (2009). *Oil Field Production Geology: AAPG Memoir 91* (1st ed.). Tulsa, USA: American Association of Petroleum Geologists.
- Soni, T. M. (2014). LPG-Based Fracturing: An Alternate Fracturing Technique in Shale Reservoirs. Bangkok, Thailand : IADC/SPE Asia Pacific Drilling Technology Conference.
- Terzaghi, K. (1942). *Theoretical Soil Mechanics*. New York: John Wiley and Sons.
- Thomson, I. (2014). CT Operations in Extended Reach Laterals – Presentation. : Halliburton Corporation.
- Valkó, P., & Economides, M. J. (1995). *Hydraulic Fracture Mechanics*. Chichester: John Wiley & Sons.
- Warpinski, N. R., Schmidt, R. A., & Northrop, D. A. (1982). In-Situ Stresses: The Predominant Influence on Hydraulic Fracture Containment. *Journal of Petroleum Technology*, pp. 653-664.
- Wasantha, P.L.P., Konietzky, H., Xu, C. (2019): Effect of in-situ stress contrast on fracture containment during single- and multi-stage hydraulic fracturing, *Engineering Fracture Mechanics*, 105: 175-189

- Wasantha, P.L.P., Konietzky, H., Weber, F. (2017): geometric nature of hydraulic fracture propagation in naturally fractured reservoirs, *Computers and Geotechnics*, 83: 209-220
- Wolgast, D., & Konietzky, H. (2014). *Verbundvorhaben PetroRes: Erschließung petrothermaler Geothermiereservoirs, Teilprojekt 2: Numerische Simulation der Risserzeugung bzw. Stimulation in geringpermeablen Gesteinsformationen im Rahmen des Multi-Riss-Konzeptes*. Freiberg: TU Bergakademie Freiberg.
- Xiong, H., Davidson, B., Saunders, B., & Holditch, S. A. (1996). A Comprehensive Approach to Select Fracturing Fluids and Additives for Fracture Treatments. Denver, Colorado, USA: Society of Petroleum Engineers, Annual Technical Conference and Exhibition.
- Yew, C. H., & Weng, X. (2015). *Mechanics of Hydraulic Fracturing* (Second ed.). Waltham: Gulf Professional Publishing.
- Yu, W., & Sepehrnoori, K. (2013). Optimization of Multiple Hydraulically Fractured Horizontal Wells in Unconventional Gas Reservoirs. Oklahoma City, Oklahoma, USA : Society of Petroleum Engineers, Production and Operations Symposium.
- Yuan, F., Blanton, E., Convey, B. A., & Palmer, C. (2013). Unlimited Multistage Frac Completion System: A Revolutionary Ball-Activated System with Single Size Balls. New Orleans, Louisiana, USA : Society of Petroleum Engineers, Annual Technical Conference and Exhibition.
- Zeeb, C., & Konietzky, H. (2014). *Entwicklung einer risikominimierten petrothermalen Explorations- und Erschließungsmethode für geeignete mitteldeutsche Kristallingesteine*. Freiberg: TU Bergakademie Freiberg.
- Zeeb, C., & Konietzky, H. (2015). Simulating the Hydraulic Stimulation of Multiple Fractures in an Anisotropic Stress Field Applying the Discrete Element Method. *Energy Procedia*, 76, 264-272.
- Zeeb, C., Schmitz, S., Barsch, M., Kleinickel, C., Kretschmar, H. J., & Konietzky, H. (2015). Simulating the Hydraulic Stimulation of a Single Fracture for EGS in a Petrothermal Environment (in press). *Geothermics, Elsevier*.
- Zeeb, C., Wolgast, D., & Konietzky, H. (2014). Simulation of Hydro-Mechanical Fracture Growth in Single- and Multi-Fracture Systems. *Veröffentlichungen des Instituts für geotechnik der TU Bergakademie Freiberg*(Heft 2), pp. 183-197.
- Zhou, L., & Hou, M. Z. (2013). A New Numerical 3D-Model for Simulation of Hydraulic Fracturing in Consideration of Hydro-Mechanical Coupling Effects. *International Journal of Rock Mechanics & Mining Science*(60), pp. 370-380.
- Zhou, L., Hou, M. Z., Gou, Y., & Mengting, L. (2014). Numerical Investigation of a Low-Efficient Hydraulic Fracturing Operation in a Tight Gas Reservoir in the North German Basin. *Journal of Petroleum Science and Engineering* 120, pp. 119-129.